TECHNISCHE UNIVERSITÄT WIEN
Vienna University of Technology

CERN

DIPLOMARBIET

Experimental Investigation of the Multipacting Phenomenon in Particle Accelerators

Roland Leber
(0928646)

Institut für Angewandte Physik

Betreuer TU Wien: Ao.Univ.Prof. Dipl.-Ing. Dr.techn. Wolfgang Werner

Projektleiter CERN: Dr. Pedro Costa Pinto, Dr. Mauro Taborelli

Einreichedatum: February 16, 2015

Abstract

The current thesis concentrates on the investigation of the Multipacting phenomenon in particle accelerators and the surface conditioning involved. In order to do so a RF resonator consisting of a wire stretched along a 1 m long part of a stainless steel beam pipe was used to initiate Multipacting and mimic the situation of a charged particle beam in an accelerator. The current of electrons impinging on the walls and the pressure rise during the Multipacting were monitored using stripe detectors and a full range gauge. After approximately 11 days of conditioning via Multipacting the surface of the beam pipe was characterized by measuring its composition by XPS and measuring the secondary electron yield (SEY). Different parameters were varied in several conditioning runs in order to optimise the surface conditioning process. Hence, the effect of superimposing the RF signal with a DC bias voltage and the effect of dodecane and acetylene injection during Multipacting were studied. In this way it was possible to prove the feasibility of reaching an SEY_{max} below 1.3, the threshold value for Multipacting in the Super Proton Synchrotron. Furthermore, a dynamic behaviour of the Multipacting over the duration of the measurement run was observed. Additional measurements regarding the effect of air exposure on the conditioned surface and the correlated change in SEY were performed.

Kurzfassung

Die aktuelle Arbeit beschäftigt sich mit der Untersuchung des Multipacting Phänomens in Teilchenbeschleunigern und der damit verbundenen Oberflächen Konditionierung. Dazu wurde ein RF-Resonator, bestehend aus einem 1 m langem Teil eines Strahlrohres aus rostfreiem Stahl entlang welchem ein Draht gespannt ist, verwendet. Der Strom an Elektronen die auf die Wand auftreffen und der Druckanstieg während des Multipactings wurden mit Hilfe eines Streifendetektors und einem Vakuummeter aufgezeichnet. Nach etwa 11 Tagen Konditionierung via Multipacting wurde die Oberfläche des Strahlrohres durch Messung der Oberflächenzusammensetzung mittels XPS und Messung der Sekundärelektronenausbeute (SEY) charakterisiert. Verschiedene Parameter wurden im Laufe dieser Arbeit variiert um die Oberflächenkonditionierung zu optimieren. Im Zuge dessen ist die Wirkung der Superposition des Hochfrequenzsignals mit einer DC-Biasspannung und die Wirkung von Dodecan und Acetylen Injektion wärend dem Multipacting untersucht worden. Auf diese Weise war es möglich nachzuweisen, dass ein SEY_{max} unter 1.3, dem Schwellenwert für Multipacting im Super Proton Synchrotron, durch Oberflächenkonditionierung mittels Multipacting erreicht werden kann. Desweiteren wurde ein dynamisches Verhalten des Multipacting über die Dauer des Messlaufs beobachtet. Außerdem ist die Wirkung von Exposition an Luft auf die Oberfläche und die damit verbundene Veränderung des SEY untersucht worden.

Contents

1 Introduction

The European Organisation for Nuclear Research (CERN), founded in 1954, operates numerous particle accelerators and related experiments, one of which is the LHC accelerator chain. The layout of the LHC accelerator chain and its experiments is schematically shown in fig. 1.1. The first chain link of the LHC accelerator chain for protons is the Linear Accelerator 2 (LINAC2) which injects the protons with an energy of 150 MeV in the Proton Synchrotron Booster (PSB). The PSB then accelerates the protons up to an energy of 1.4 GeV and passes them on to the Proton Synchrotron (PS). The PS reaches proton energies of 26 GeV. After the PS the protons reach the Super Proton Synchrotron (SPS), the last chain link before the LHC, which accelerates the protons up to 450 GeV. After the SPS the protons finally reach the Large Hadron Collider (LHC) where they are accelerated up to 3.5 TeV before the upgrade of 2013/2014 and up to 7 TeV after the restart in 2015. These accelerators provide the proton beam for a variety of experiments, not only for the four LHC experiments ATLAS, LHCb, CMS and ALICE, but also other experiments like the Isotope mass Separator On-Line facility (ISOLDE) supplied with protons from the Booster or the COmmon Muon Proton Apparatus for Structure and Spectroscopy (COMPASS) experiment receiving its protons from the SPS [12].

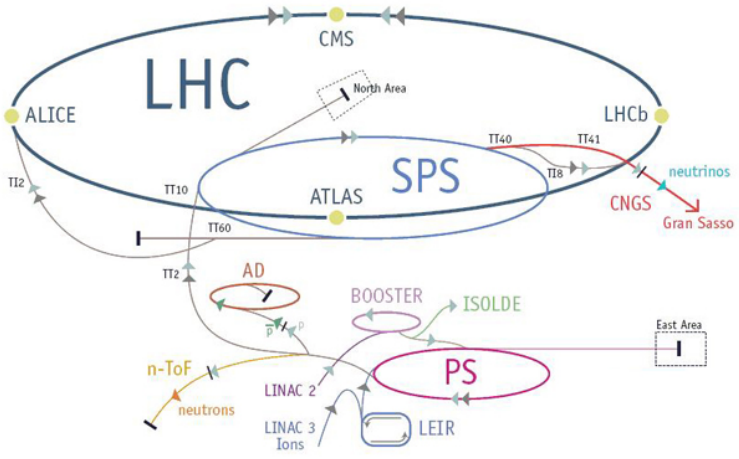

Figure 1.1: Schematic representation of the LHC accelerator chain [12].

The present thesis focuses on the study of the Multipacting phenomenon and on surface conditioning as a possible way to mitigate the related e-cloud build up in particle accelerators. The first beam instability related to Multipacting was observed in 1965 in a small storage ring at INP Novosibirsk. Until today the Multipacting phenomenon has been observed in numerous accelerator facilities all over the world, for example at the Bevatron in Berkeley and the Los Alamos PSR and became a major concern within the accelerator community. At CERN Multipacting was the first time observed at the Intersection Storage Rings (ISR) in 1972 [13].

For the year 2018 a major upgrade of the LHC accelerator chain is foreseen to increase the luminosity. In order to do so the LINAC2 will be replaced by the LINAC4 [27]. The new beam parameters foresee an increase of the bunch population from 1.15×10^{11} to 2.2×10^{11} with a bunch spacing of 25 ns or even 3.5×10^{11} protons per bunch with a bunch spacing of 50 ns [2]. In order to profit from this intense beam it is necessary to further suppress Multipacting in the SPS. Problems caused by the electron cloud in the SPS are transverse emittance blow-up along the batch, dynamic pressure rise due to electron stimulated desorption, septum sparking and enhanced beam dump outgassing. First tests at the end of 2014 already showed that big improvements regarding the Multipacting phenomenon have to be made since high losses were observed during the test at high beam intensity and therefore it was impossible to reach the beam parameters required for LHC injection. To reduce Multipacting in the SPS different approaches were under investigation, for example clearing electrodes, grooves and special surface treatments [3]. The present work focuses on the reduction of the Multipacting via in-situ surface modification through surface conditioning. Surface conditioning would be the method of first choice, since other methods pose big challenges. For example, in order to coat the SPS chambers with carbon it would be either necessary to transport approximately 700 dipole and 200 quadrupole magnets to surface and coat them within one year or develop a coating system that can be operated directly in the SPS tunnel without removing the magnets from the tunnel. Furthermore during the present work also the behaviour and the build up of the e-cloud was studied in order to gain a better understanding on how to mitigate this phenomenon in the LHC and other accelerators.

2 Principles of Multipacting and its mitigation by coatings

2.1 Secondary-Electron Emission

Secondary electron emission is a process already known since the early 20. century and plays an important role for many modern technologies. For electron multipliers or cathodes in crossed-field devices materials are used with a high Secondary Electron Yield (SEY) to achieve a fast multiplication of the primary electrons, whereas for other applications like the inner wall coatings of particle accelerators and waveguide filters [20] in satellites it is crucial to use a material with a low SEY.

The total SEY is defined as the ratio between emitted $I_{emitted}$ and impinging $I_{primary}$ electrons:

$$\delta = \frac{I_{emitted}}{I_{primary}} \tag{2.1}$$

but mostly the equation:

$$\delta = \frac{I_{primary} - I_{sample}}{I_{primary}} \tag{2.2}$$

where I_{sample} is the current measured at the sample, is used [29].

The process of secondary electron emission can be divided into three steps: (1) excitation of an electron by an impinging primary electron, (2) transport of the secondary electron from the sample bulk to the surface and (3) escape of the secondary electron by overcoming the surface barrier [28]. Most theories for describing secondary electron emission are based on the power-law theory, the following explanation is based on ref. [30]. In power-law theory for the calculation of the SEY δ the equation:

$$\delta = \int n(x, E_0) f(x) dx \tag{2.3}$$

is used, where $n(x, E_0)$ is the number of secondary electrons produced by a primary

electron between a depth x and $x+dx$ with the energy E_0. $f(x)$ is the escape probability of the secondary electron. $n(x, E_0)$ is given by:

$$n(x, E_0) = -\frac{1}{\epsilon}\frac{dE}{dx} \tag{2.4}$$

where ϵ is the energy required to produce a secondary electron and $-dE/dx$ is the so called stopping power, i.e. the energy loss per unit length of the primary electron while passing through the sample. To express $f(x)$ one needs to consider that only a fraction of the excited electrons moves towards the surface and not every electron that reaches the surface is able to overcome the surface-vacuum barrier, this is considered by the coefficients B_1 and B_2. So $f(x)$ can be written as:

$$f(x) = B_1 B_2 e^{-x/L} \tag{2.5}$$

where L is the effective escape depth. To gain an explicit expression for the SEY further assumptions regarding the term $-dE/dx$ have to be made. So the energy loss per unit path length is considered approximately constant throughout the primary-electron range R. The primary-electron range can be expressed as:

$$R = \frac{1.15 \times 10^{-6}}{\rho} E_0^{1.35}\,[cm] \tag{2.6}$$

where ρ is the density of the sample in g/cm^3 and E_0 is given in keV. Now the expression:

$$-\frac{dE}{dx} = \frac{E_0}{R} \tag{2.7}$$

can be obtained. By using eqs. 2.4, 2.5, 2.7 in eq. 2.3 the searched explicit expression for the SEY can be obtained:

$$\delta = \int_0^R \frac{B_1 B_2}{\epsilon}\frac{E_0}{R} e^{-x/L} dx = \frac{B_1 B_2 E_0 L}{\epsilon R}(1 - e^{-R/L}) \tag{2.8}$$

Fig. 2.1 shows a typical SEY curve, the form of the curve can be easily explained. With increasing energy of the primary electrons the penetration depth increases. As long as the penetration depth is lower than the escape depth of the secondary electrons a majority of the secondary electrons can escape. So until the penetration depth equals the escape depth the SEY rises. If the penetration depth of the primary electrons exceeds the escape depth of the secondary electrons, the SEY decreases. This behaviour is due to the fact that the primary electrons loose most of their energy at the end of their trace and so the majority of the secondary electrons are excited deep inside the bulk and are

not able to reach the surface-vacuum interface [28]. The fact that the primary electrons loose most of their energy at the end is not considered in the derivation above since it is simplified by using a constant energy loss per unit path length.

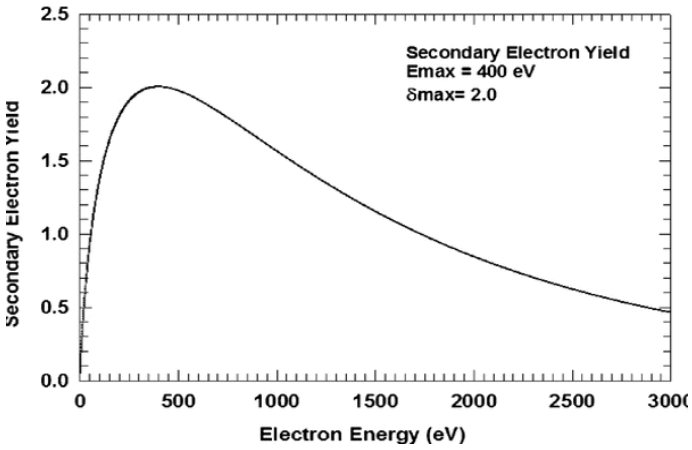

Figure 2.1: A typical SEY curve [19]

The SEY is also influenced by the incident angle of the primary electrons. So the SEY value and the energy at which the maximum SEY occurs (E_{max}) increases with the angle relative to the sample's normal. For example E_{max} of clean molybdenum equals 490 eV for $\theta = 0\,^\circ$ and 660 eV for $\theta = 60\,^\circ$ [28]. The SEY increases with increasing incident angle, since by increasing the angle of incidence the penetration depth decreases and so the secondary electrons are produced closer to the surface. Therefore, a higher number of secondary electrons can reach the surface-vacuum interface.

The SEY depends very strongly on the material: most clean metals exhibit an SEY between 0.5 and 1.8 and insulators an SEY of 5 and above. This is due to the difference in the escape depths of secondary electrons for different materials, metals typically have a small escape depth (e.g. 30 Å) and insulators a long escape depth (e.g. 200 Å). This can be explained by taking a look at the band structure. Insulators are characterised by a large band gap, therefore a higher kinetic energy of the secondary electrons is necessary to undergo energy losses through elevating electrons from the Fermi level to the unoccupied states of the conducting band. In metals on the other hand the density of states in the conducting band is high; therefore the secondary electrons loose a lot of energy due to electron-electron interactions [30].

Table 2.1: Measured maximum SEY values of different materials [29].

	δ_{max}
C	0.9
Ag	1.5
Mo	1.2
W	1.4
Cu	1.3

The SEY depends mainly on the surface properties of a material and therefore it is very strongly affected by the surface composition. Since most of the materials used in technology tend to build oxide or adsorbate layers one always has to consider the change in the SEY after air exposure. In most cases this leads to a strong increase in the SEY. For example the SEY of clean copper increases from 1.3 to about 2 after air exposure [1]. In the following materials after air exposure are referred to as technical materials.

2.2 Multipacting

Multipacting is a limiting factor for Radio Frequency (RF) devices such as cavities, RF tubes, RF couplers and also for particle accelerators with a positively charged beam. RF devices and particle accelerators show a similar Multipacting behaviour since the particle beam used in particle accelerators consists of particle bunches with a bunch spacing of a couple of ns and therefore causes an electric field similar to an RF field [21].

There are two kinds of Multipacting, single-surface Multipacting and two-surface Multipacting. The single-surface Multipacting process is in general started by a free electron in an RF field normal to the surface of the RF device. When the electron hits the surface secondary electrons are emitted which are again accelerated by the RF field. If this process repeats itself always at the same RF phase only in a later RF cycle this causes an avalanche of electrons [14]. As shown in fig. 2.2, two-surface Multipacting is started by a single electron (e. g. a photoelectron) that is accelerated towards the wall by the periodic changing electric field caused by the particle beam. When the electron hits the wall secondary electrons are emitted and if the emission process is in resonance with the electric field, the secondary electrons are accelerated again and cause more secondary electrons. This leads to an exponential multiplication of the electrons [11].

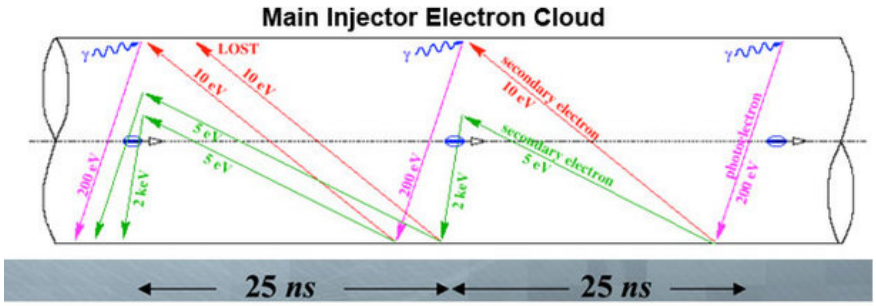

Figure 2.2: Schematic representation of the Mulipacting phenomenon [11]

For Multipacting development two conditions need to be fulfilled. Firstly, in the case of short gap cavities, the time between two impacts has to be an integer number of the half period time of the RF field, because this means that the new generated electrons always have the same conditions and this leads to a self-sustaining electron cloud. However, for the field geometry discussed in the present thesis the time between two impacts has to be an integer number of the full period time in order to always have the same conditions for the acceleration of the secondary electrons. To fulfil this condition in a short gap cavity the following equations have to be valid. The time t in between two impacts needs to be:

$$t = \frac{1}{2\nu}(2n-1) \tag{2.9}$$

where ν is the RF frequency and n is the order of the Multipacting discharge. Eq. 2.9 is fulfilled if the amplitude of the electric field E with the frequency ν equals:

$$E = 4\pi\frac{m_0c^2}{e}(\frac{L}{\Lambda})^2\frac{1}{(2n-1)} \tag{2.10}$$

where L is the distance between the two facing walls and Λ is the RF wavelength. The kinetic energy of the impinging electron is then given by:

$$E_{kin} = 8m_0c^2(\frac{L}{\Lambda})^2\frac{1}{(2n-1)} \tag{2.11}$$

Secondly the SEY of the surface needs to be high enough to produce more secondary electrons than primary electrons are absorbed [21].

There are three ways to suppress Multipacting, firstly since the multiplication factor

Y is given by:

$$Y = \delta^N \tag{2.12}$$

one can use a material with a low SEY (below or near one). This is the possibility on which we will focus during the current thesis and is in our case achieved by applying carbon coatings or by surface conditioning. The second way to suppress Multipacting is to avoid spatial focusing and resonant build-up. This method uses an axial electric DC field to change the trajectories of the electrons and destroys in this way the synchronisation of the electron multiplication with the RF field or the electric field of the particle beam. Furthermore, in this way also the impact energy of the primary electrons can be shifted from an energy regime with high SEY to an energy regime with lower SEY [21]. The third way of suppressing Multipacting is to use the magnetic field of a solenoid in order to destroy the synchronisation with the RF field [6].

2.3 Surface Conditioning against Multipacting

Since the inner walls of the particle accelerators are exposed to air during construction and due to the need to vent the accelerator from time to time for maintenance it is not possible to maintain a clean metal surface. Due to the high SEY of technical metal surfaces an interest in in-situ treatments arose. An in-situ treatment of the inner walls can be achieved by using the so called conditioning or beam scrubbing effect [26].

During conditioning the effects of Multipacting on the surface are used to lower the SEY. The impinging electrons cause electron stimulated desorption and this leads to a decrease of the SEY due to the cleaning of the surface. Furthermore, carbonaceous film growth on the metal surface is initiated by the impinging electrons. The results of different investigations suggest that the carbon responsible for the film growth might not come from the residual gas present in the chamber. Furthermore, it is assumed that the carbon responsible for the film growth might diffuse out of the bulk to the surface [15] [17]. For example, measurements on clean silicon [26] and on the aluminium alloys 1100 and 6063 [22] showed no carbonaceous film growth. The aluminium alloys even showed an increasing SEY after a longer conditioning period due to the revealing of aluminium oxide on the surface which was initially covered by adsorbates caused by air exposure.

At the beginning of the conditioning process a fast decrease in the electron stimulated desorption yield can be monitored, accompanied by a decrease in the electron yield. During the electron stimulated desorption mainly H_2, H_2O, CO and CO_2 are released. After a certain received electron dose the electron stimulated desorption yield reaches a

constant value and the decrease in the SEY is mainly due to a constant carbonaceous film growth [15]. The carbonaceous film growth makes it possible to reach SEY values below the SEY of the clean metal.

2.4 Hybridization of Carbon

Carbon is a material of major interest for SEY mitigation since, depending on its allotorpe, carbon is featured with an SEY of below 1. Carbon is the sixth most common element in the universe and it is essential for every form of life on earth. Furthermore, its allotropes are widely spread through a broad field of technological applications, for example diamonds are used due to their extreme hardness for cutting, polishing and drilling and graphite is used to reduce friction [7].

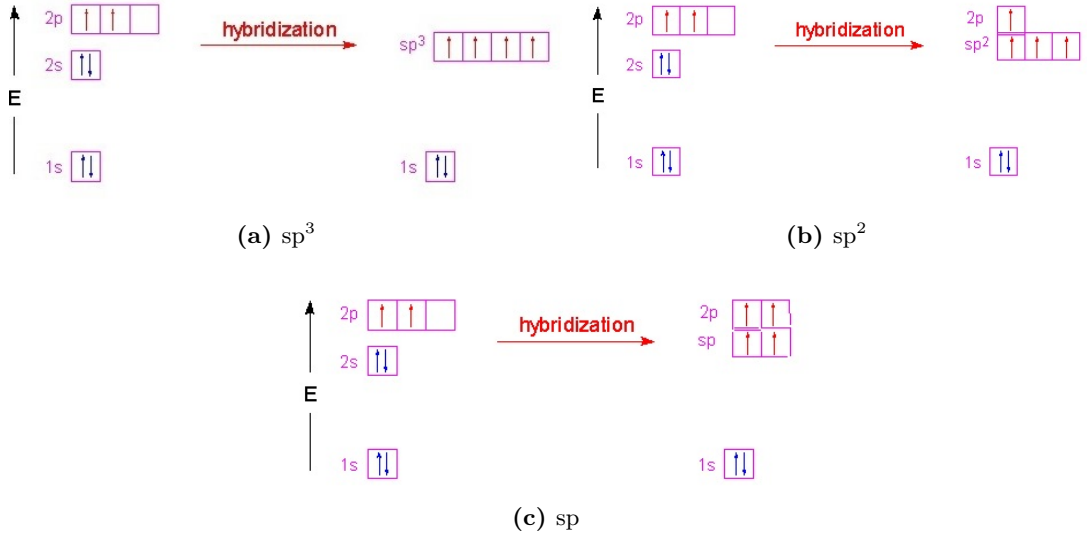

(a) sp^3 **(b)** sp^2

(c) sp

Figure 2.3: Schematic representation of the three different kinds of carbon hybridization [5].

Carbon is such a versatile element due to its three kinds of hybridization [8], shown in fig. 2.3. Carbon can form sp^3 hybrid orbitals combining the 2s orbital with all three 2p orbitals. Carbon in the sp^3 hybridization develops a tetrahedral geometry with an angle of 109.5° in between the orbitals. Diamond is one structure in which carbon forms sp^3 hybrid orbitals. Another possible hybridization of carbon is the sp^2 hybridization which combines the 2s and two 2p orbitals. Carbon in the sp^2 state posseses a trigonal planar structure with an angle of 120° in between the orbitals. sp^2 hybridization is formed in Graphite and other carbon molecules with double bonds. Carbon is able to form a third

kind of hybridization, the sp hybridization giving rise to triple bonds. In order to form the sp hybridization the 2s orbital combines with one of the 2p orbitals.

2.5 Hollow Cathode Sputtering

For the production of thin films in industry deposition rate and costs are two main key factors and so it is always desired do improve these factors while maintaining the quality of the coating. Hollow Cathode Sputtering (HCS) is a technique that makes it possible to achieve, compared to classical magnetron sputtering, relatively high deposition rates at low costs.

In the case of classical glow discharges electrons are emitted by the cathode, accelerate while passing the potential drop near the cathode, ionise the working gas in the negative glow and continue straight towards the anode. In the hollow cathode design the cathode faces another cathode. In this way the electrons are accelerated during the cathode drop until they feel the field of the opposite cathode. This leads to an oscillating movement of the electrons. Fig. 2.4 schematically shows the design of a hollow cathode. The electrons oscillate between the cathodes until they have lost most of their energy and then they move towards the anode [18].

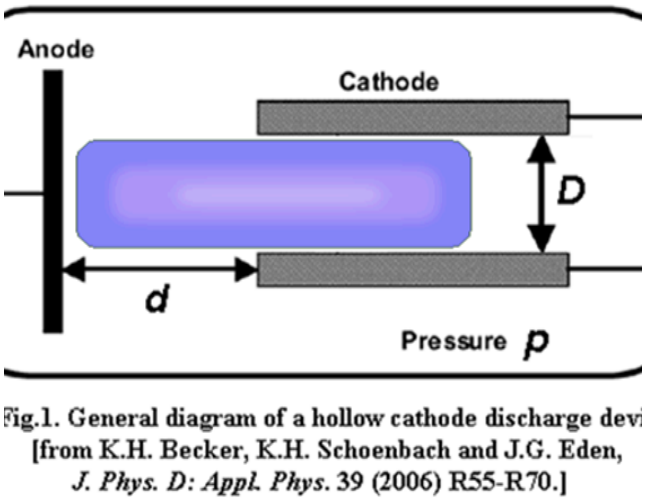

Figure 2.4: Schematic drawing of a hollow cathode discharge device [10].

The design of hollow cathodes can be very well adjusted to one's needs. Simple hollow cathode configurations exist which use a cylindrical geometry, but as shown in fig. 2.5 there are also flat targets with complicated slots and bores for large area de-

position. Depending on the geometry of the target a gas flow through the target or a substrate/cathode movement is needed [18]. In some configurations the plasma discharge can be further improved by applying a magnetic field [24].

Figure 2.5: The figure shows an example for a hollow cathode design [16].

Using HCS has numerous advantages. It is for example often possible to use more than 90 % of the target material, due to the high plasma uniformity. In comparison, a normal magnetron sputter system uses 25-30 % of its target material due to the inhomogeneous magnetic field and the connected non-uniform erosion. Furthermore due to the geometry of hollow cathodes the sputtered material either coats the substrate or redeposits at the target. This reduces material and maintenance costs. Due to the higher number of ionisation processes per free electron it is possible to work with lower working gas pressures compared to a diode discharge. By using a cylindrical cathode it is also possible to coat all sides of a three dimensional object simultaneously with a deposition rate of hundreds of angstroms per second. Finally, is it possible to build industrial HCS systems with which a high number of objects can be coated within a short time [24].

3 Experimental

3.1 Multipacting Test Bench

In order to investigate the Multipacting process in particle accelerators and to search for the ideal parameters to achieve a maximum conditioning effect a special Multipacting test bench, represented in fig. 3.1, was developed. In this test bench Multipacting can be stimulated by using an RF signal. This gave us the freedom to be independent of machine development runs of the accelerator and also the possibility to experiment with additionally injected hydrocarbons.

Figure 3.1: Image of the Multipacting test bench.

Fig. 3.2 schematically shows the main components of the test bench. Inside the test bench the electric field related to the RF signal and the superimposed DC bias voltage accelerates free electrons preferentially in the direction of the magnetic field. In this way a similar e-cloud build up as in the SPS can be achieved. Stripe detectors are used to monitor the Multipactig current. By measuring the current rise during the power ramp and the electron dose per shot either over the length or the with of the liner information about the e-cloud distribution and its dynamic behaviour can be acquired. Furthermore, a Residual Gas Analyser (RGA) and a penning gauge are used

to gain information about the pressure rise and the kind of gases released due to the electron stimulated desorption caused by the Multipacting. To investigate the effect of the electron cloud on the surface composition and the related SEY sample stripes are mounted on one side of the liner facing the stripe detector. In this way it is possible to directly relate the current measured at the stripe detector to the corresponding sample. These sample stripes are afterwards measured with the SEY/XPS system. It is desired to gain in this way a better understanding of the e-cloud build up, its behaviour over time and an the correlated surface conditioning.

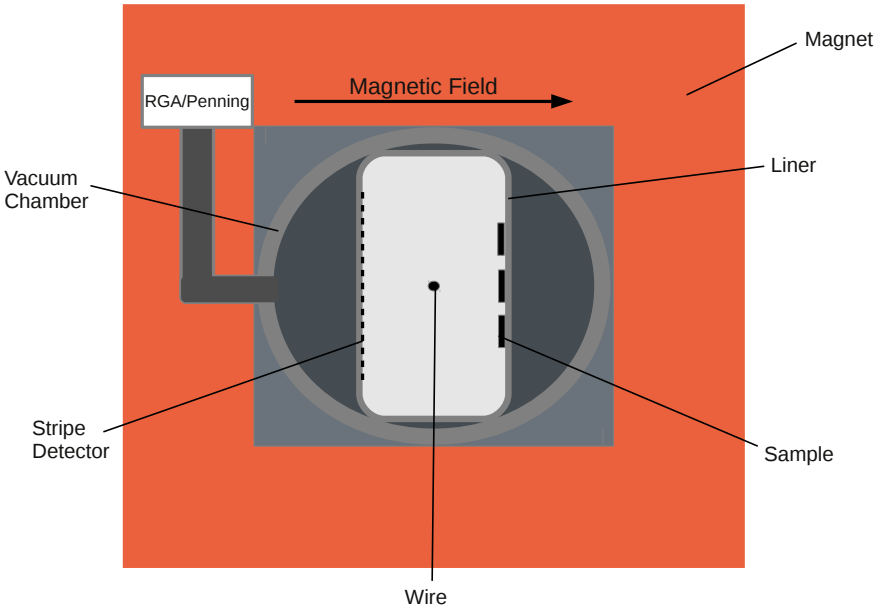

Figure 3.2: Schematic drawing of the multipacting test bench set up.

3.1.1 Vacuum System

The Vacuum system consists of a 1.4 m long chamber featured with an RGA (Prisma QMS200) and a full range pressure gauge(Pfeiffer IKR270). During the Multipacting runs a 1 m long beam pipe called liner was inserted into the vacuum chamber as for the electron cloud monitors of the SPS. One liner as used in the Multipacting test bench is shown in fig. 3.8. The liners are manufactured from stainless steel 316LN and have the same cross section as the chambers of the MBB SPS dipoles. The pumping group uses a turbomolecular pump and a roughing pump and is able to reach a base pressure down to the high 10^{-8} mbar range. Furthermore the vacuum system is featured with a

gas injection line used to inject hydrocarbons during the Multipacting run. In order to reproduce the same conditions as in the SPS, which cannot be baked, the Multipacting test bench was only baked after using carbonaceous gases. During the bake outs no liner was inserted and the system was vented before starting the next Multipacting run.

3.1.2 RF System and Data Acquisition

The main part of the RF system is the resonator consisting of the vacuum chamber, the liner and a tungsten wire stretched along the central axis of the vacuum chamber and the liner. The resonator is inserted into an MDHW dipole as used in the electron cloud monitors installed in the SPS. The RF signal is generated by a Vector Network Analyser (VNA) (Rohde & Schwarz® ZNB4) and goes to the amplifier (Herfurth® HV 50 E 30-200) which amplifies the signal up to 40 W. A directional coupler is used to separate the incoming RF signal from the reflected RF signal. A DC block protects the amplifier and VNA from the DC bias voltage applied at the tungsten wire. The RF matching and the bias voltage are applied directly in front of the resonator. The end of the resonator (the wire) is short circuited by two capacitors. The resonance frequency of the resonator is approximately 95 MHz (fig.3.4). The RF system is represented in fig. 3.3.

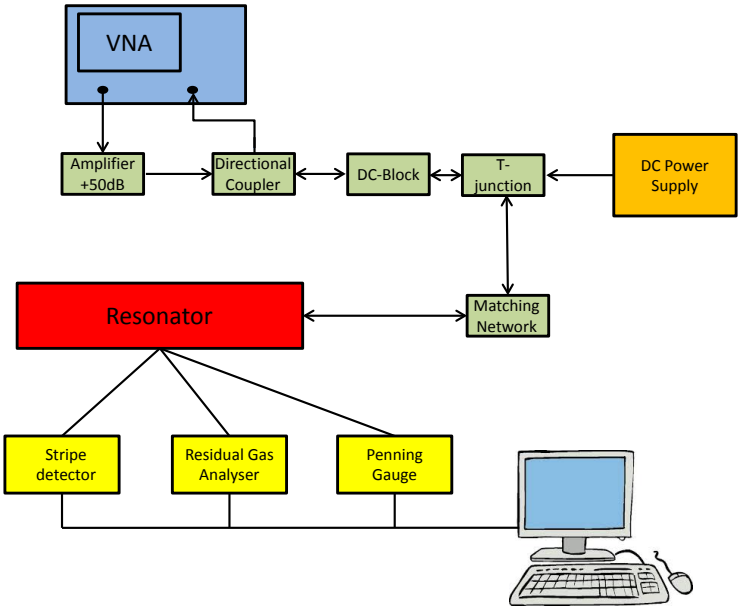

Figure 3.3: Schematic representation of the RF and data acquisition system

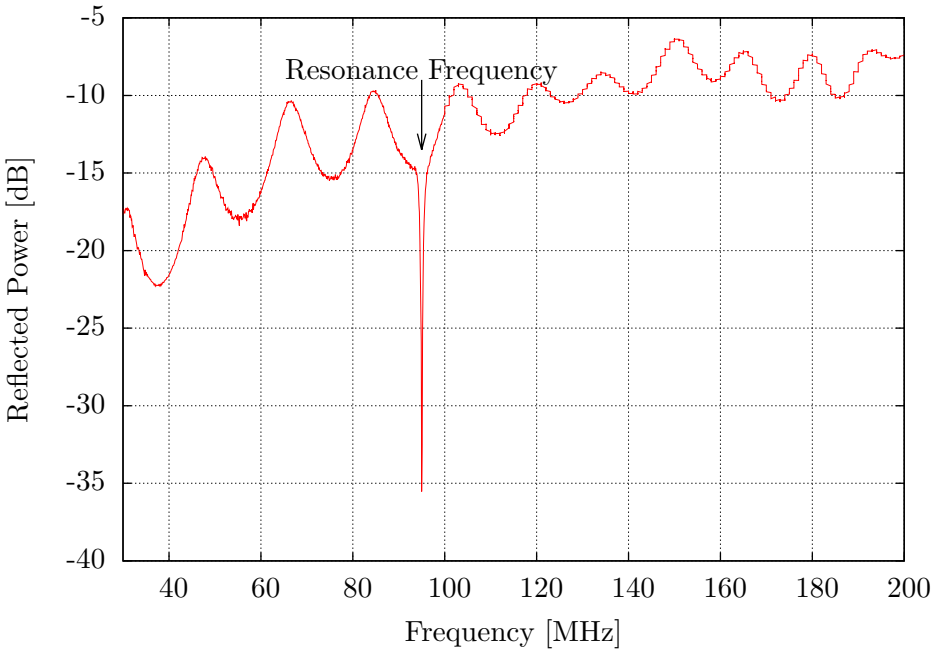

Figure 3.4: Frequency sweep from 30 MHz to 200 MHz in 20 kH steps with the resonance frequency at 95 MHz.

To acquire information about the electron distribution inside the liner stripe detectors with longitudinal and transversal stripes are used. The liner has holes with a diameter of 2 mm along one side and a total transparency of 7%, since this value proved to be small enough to not take effect on the Multipacting build up. In order to avoid the emission of secondary electrons from the stripe detector a positive potential of 9 V is applied to the stripes. The stripe detectors are made out of 0.1 mm thick Kapton with electro plated copper stripes on top. The stripes of the longitudinal stripe detector are 2 mm wide with 0.17 mm spacing in between two stripes. The stripes of the transversal stripe detector are 8 mm wide with the same spacing in between the stripes as the longitudinal stripe detector. The stripe detectors are featured with 47 copper stripes plus one ground. The 47 stripes are bundled to 16 channels. Channel 1 to 15 contain 3 stripes each and channel 16 only 2 stripes. Fig. 3.5 shows the CAD drawings for the stripe detectors.

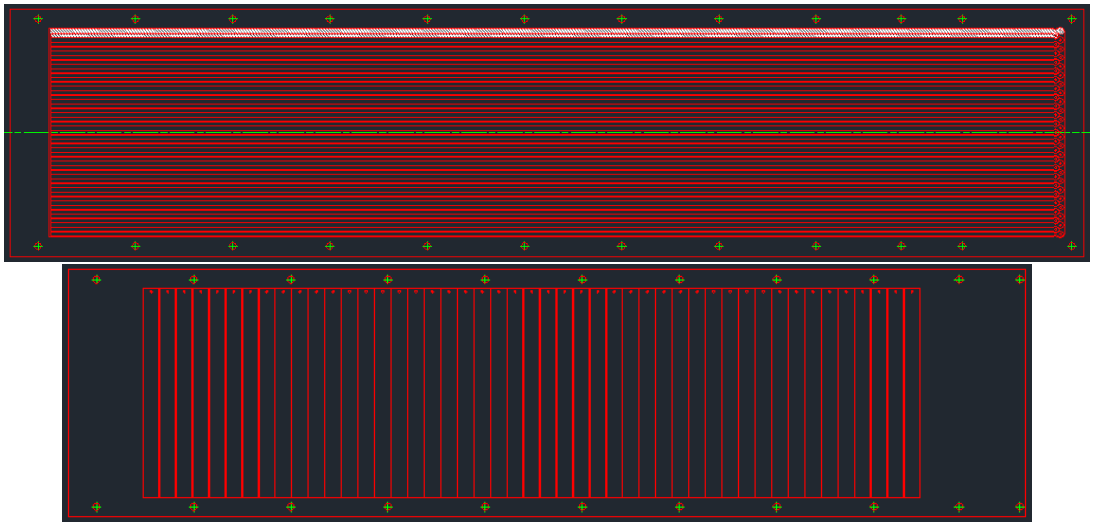

Figure 3.5: CAD drawings of the stripe detectors with longitudinal and transversal stripes.

The current is monitored by the data acquisition system (National Instruments® USB 6221). In order to measure the signal from the stripe detector the data acquisition system transforms the current to a voltage by using 100 kΩ resistors. The data is then processed by a LabVIEW® programme. The LabVIEW® programme triggers automatic shots every 120 s and monitors the pressure and the current signal. The programme saves the pressure and the current of one shot every 30 shots in ASCII format.

3.1.3 The Retarding Field Energy Analyser

In order to measure the electron energy distribution of the e-cloud with different DC bias voltages trials with a Semmion Single Sensor® from Impedans were carried out, but the electron flux proved to be below the detection limit of the probe. Hence, a special Retarding Field Energy Analyser (RFEA) was designed with a higher transmission and a larger sampling area. The design of the analyser was optimised using the finite element method simulation software Opera®. The simulations were used to minimize the error caused by the deviation of the actual minimum pass energy from the desired minimum pass energy.

The simulations showed that using only one retarding grid and one grid on ground leads to an error of 37 % due to the potential drop in the holes. So in order to reduce the potential drop to a minimum two retarding and two grids on ground proved to be the best solution. For the final design a 1 mm spacing between the two retarding grids, the two grounded grids and the second retarding grid and the collector plate was chosen

and a 2 mm spacing between the second grounded grid and the first retarding grid. This design showed a deviation of only 4.8 % of the actual minimum pass energy from the desired one.

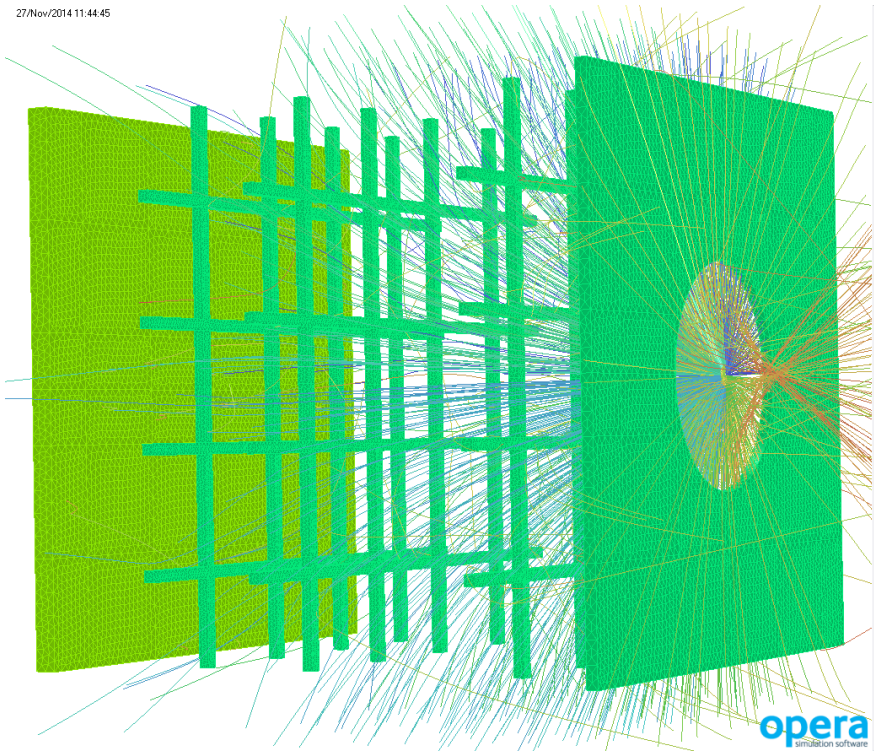

Figure 3.6: Simulated electron trajectories in one hole of the RFEA, an SEY of 0.95 (SEY of the carbon coatings) was assumed for all surfaces, the retarding voltage was set to -200 V and the collector voltage to +9 V. As emitter a hemisphere in the centre of the hole of the first grid was used, the energy of the primary electrons was set to 250 V with a flux density of $5.0 * 10^{-3}$ A/cm^2.

The error values of selected simulations are given by tab. 3.1 and the simulated error curve in 25 V retarding voltage steps is represented by fig. 3.7 left. The simulated error curve showed an inaccuracy due to the potential drop in the holes of 5.6 % for a retarding voltage of 25 V and decreases to 4.7 % at 250 V and above. A simulation with consideration of the space charge and the emission of secondary electrons emitted by the grids and the collector plate showed that the negative voltage of the retarding grid and a positive voltage of 9 V on the collector plate is sufficient to suppress losses due to the secondary electrons. The result of the simulation is represent by fig. 3.6.

Table 3.1: Selection of simulations carried out in order to optimise the design of the RFEA, for all simulations a retarding voltage of -200 V and a collector voltage of +9 was used. GS stands for grid spacing, R for retarding grid, G for grid on ground and C for collector plate. The max error of electrons passing through gives the deviation of the lowest kinetic energy at which the electrons are able to pass through the centre of the grid from the energy they are supposed to be able to pass. The parameters chosen for the final design are highlighted in grey.

Number of grids on ground	Number of retarding grids	GS between G and R [mm]	GS between R and C [mm]	GS between R and R [mm]	GS between G and G [mm]	Max error of electrons passing through [%]
1	1	1	1	-	-	37.00
1	1	2	1	-	-	27.50
1	1	3	1	-	-	21.45
1	1	2	2	-	-	21.60
1	2	2	1	1	-	11.00
1	2	2	1	2	-	8.15
2	2	2	1	1	1	4.80

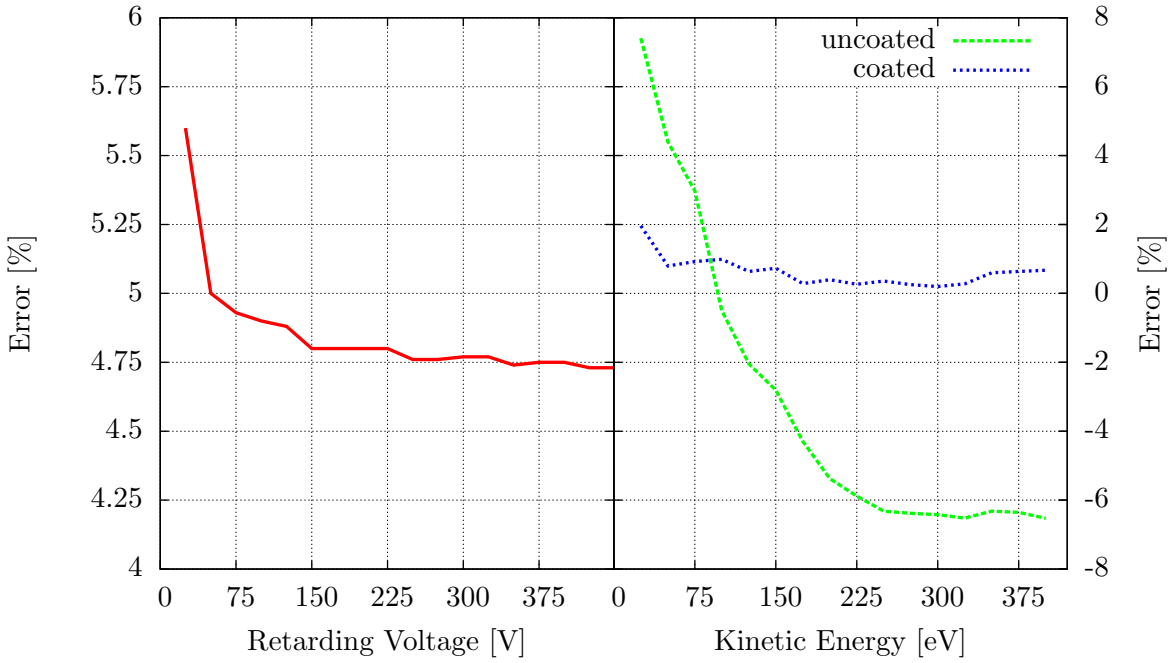

Figure 3.7: Simulated error curve for different retarding voltages in 25 V steps left and measured error curve in 25 eV steps right.

In order to test the accuracy of the final RFEA design a small testing chamber was built in which a flood gun (Specs FG 15/40) was used to shoot electrons with a given energy in a normal angle on the RFEA. The energy of the electrons was varied in 25 eV

steps from 25 to 400 eV. 400 eV is the maximum kinetic energy since the electronics of the Semmion® used for data acquisition and controlling the self build RFEA has a maximum retarding voltage of 420 V. The error of these measurements is defined as the deviation of the electron energy of the maximum of the energy profile from the electron energy set at the flood gun.

The measured error curve for uncoated retarding grids and collector plate, given by fig. 3.7 right green curve, shows the combined error of the delivered energy of the flood gun and the RFEA of +7.4 % for electrons with a kinetic energy of 25 eV and changes to a stable error of around -6.5 % for energies above 250 eV. The highest accuracy was observed for electrons with a kinetic energy of around 100 eV with an error of only 0.5 %. For low energies the error is dominated by the potential drop in the holes, the reason for the positive error for higher energies might be the contribution of secondary electrons emitted by the retarding grids. In order to further improve the resolution of the analyser the collector plate and the two retarding grids were coated with carbon to suppress secondary electron emission. The error measurements for the coated RFEA decreased to below 1 % for kinetic energies higher than 25 eV. The measured error curve is given by fig. 3.7 right blue curve.

3.1.4 Measurement

Before every measurement a fresh cleaned liner is introduced into the Multipacting test bench. The liner is featured with three additional stainless steel stripes (fig. 3.8) along the stripe detector as samples for the SEY/XPS measurements. The Multipacting runs to study conditioning last approximately 11 days. During the Multipacting run 30 s power ramps (shots) are applied with a 90 s delay in between. Around 7900 shots per Multipacting run are applied. The RF frequency during the shots is chosen in such a way that the ratio between input power and reflected power is ca. -27 dB. The signal of the pressure gauge and the stripe detector is saved once an hour (every 30 shots) by the LabVIEW® programme. Three times per day manual shots are applied in order to also save the reflected power.

Figure 3.8: Image of the three sample stripes mounted on a liner facing the stripe detector.

3.1.5 Evaluation of the data

During one measurement run the pressure and Multipacting - current development during hundreds of shots are saved. Since processing such a large number of files manually would require a lot of time, MATLAB® programmes are used. The MATLAB® programmes are used to find and calculate the following values from the data files:

- P_{delta} (difference between base pressure and maximum pressure during the shot)
- I_{max} (maximum current of each channel per shot)
- Global I_{max} (maximum current of all channels during the shot)
- D (electron dose accumulated during one shot per channel)
- Average D (dose averaged over all channels)
- $D_{cumulative}$ (sum over the electron doses per shot over the lenght of the measurement)
- Average $D_{cumulative}$ (cumulative dose averaged over all channels)

The dose D_j^i per saved shot j and channel i is defined as:

$$D_j^i = \frac{\sum_{t=0}^{30} I_t^i * \Delta t}{A * 0.07} \tag{3.1}$$

where I_t^i is the current of channel i at time t saved once per second, Δt is the duration of the current value (1 s in our case) and A the area of two/three stripes multiplied with 0.07 to correct for the transparency of the liner. Furthermore, the cumulative dose is calculated manually by summing up the dose per shot over the whole run. Since only the data of one shot every 60 min is saved the shots in between are approximated by using the mean value of two sequent files and multiplying it by 30 for the number of shots in between two saved files (eq. 3.2, J corresponds to the total number of shots saved).

$$D^i_{cumulative} = \sum_{j=0}^{J} \frac{D^i_{j-1} + D^i_j}{2} * 30 \tag{3.2}$$

3.1.6 Cleaning procedure of the liners

In between two measurements the liners are degreased and etched to remove the carbon layer achieved through surface conditioning. For the degreasing the detergent NGL Cleaning Technology 17.40 spec. ALU III in a concentration of 10-20 g/l is used. The liners are put in a bath of this detergent with a temperature of 45-55 °C for 1-3 h and are agitated by ultrasound for 10-20 min at a frequency of 25 kHz. After the degreasing the liners are rinsed with a tap water jet. Following the rinsing the liners are put into the etching bath for 30 min. For the etching a solution consisting of 30-50% Nitric acid and of 5% Hydrofluoric acid is used. During the experiments it was discovered that the 30 min etching time is not always sufficient in order to completely remove the carbon layer on top, this lead to a lack of reproducibility of the measured results. This was especially observed after the run with dodecane injection, therefore for future experiments the etching time will be increased to 3 h. After the etching the liners are again rinsed with a tap water jet, then with a demineralised water jet and cleaned with ethanol to facilitate the subsequent drying. Then the liners are dried by using a nitrogen or filtered compressed air flow and baked by using a hot air flow at 60 °C for 10-60 min.

3.2 Coating System

Direct Current Hollow Cathode Sputtering (DCHCS) was chosen for the carbon coatings for SEY mitigation applied to the SPS dipoles for a variety of reasons. During previous research, coatings were applied to SPS dipoles by Direct Current Cylindrical Magnetron Sputtering (DCCMS), by Plasma Enhanced Chemical Vapour Deposition (PECVD), by Direct Planar Magnetron Sputtering (DCPMS) and by DCHCS. For DCCMS it would be necessary to remove the beam pipe from the magnet during the coating and insert it

afterwards again. The carbon coatings applied by PECVD possessed a maximum SEY greater than 1.3 (measured value 1.5), this might be due to the lower surface roughness or a higher hydrogen concentration within the coating. DCPMS was tested by using the magnetic field of the dipole itself and by using permanent magnets. Using the magnetic field of the SPS dipole itself did not work, because of the wrong orientation of the magnetic field and using permanent magnets resulted in a non-uniform coating. DCHCS proved to be the best choice for coating the SPS dipole chambers, since it makes it possible to coat the SPS dipoles without disassembling them and it produced the most uniform coating compared to the other investigated techniques. A more detailed report on this topic can be found in ref. [23].

In order to compare the results obtained by the Multipacting test bench to the Multipacting behaviour in the SPS, it is necessary to determine the threshold SEY at which Multipacting can be initiated in the Multipacting test bench. The SEY threshold of 1.3 for the SPS was theoretically calculated. In order to do so carbon coatings with different SEY were produced and will be inserted into the Multipacting test bench at a later time. The SEY of the carbon coatings was altered by adding small amounts of hydrogen to the working gas during the coating.

For the coatings discussed in the current thesis the pumping group and the power supply used for coating the SPS dipoles were connected to a smaller chamber, which was adapted to coat the one meter long liners used for the Multipacting test bench.

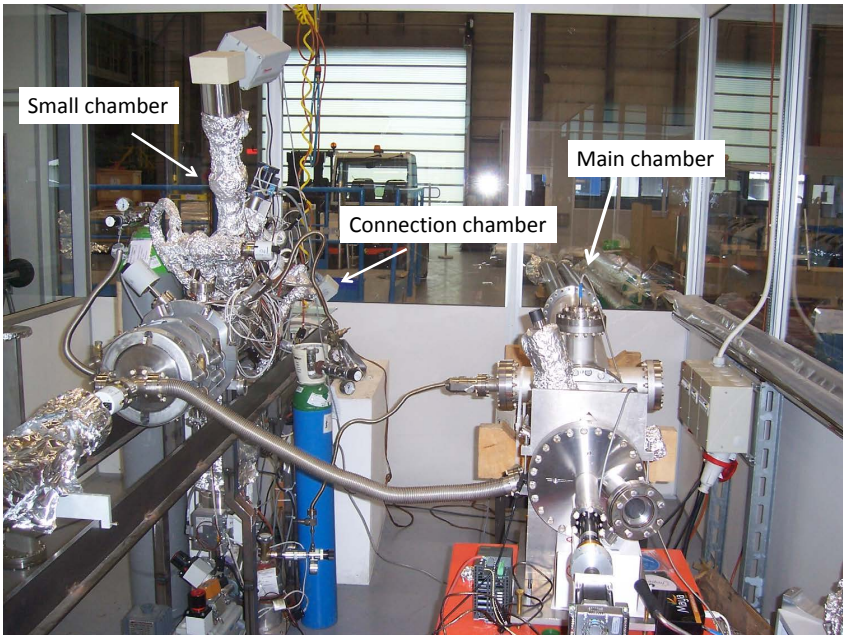

Figure 3.9: Image of the coating system

The coating system used for the production of the carbon coatings with different SEY is represented in fig. 3.9 and fig. 3.10. The system consists of three chambers, the main chamber houses the liner and the cathode, the connection chamber that is connected to the gauges and the main pumping group and one small chamber which has its own pumping group and a Residual Gas Analyser (RGA). The two pumping groups consist each of a turbo-molecular pump and a rotary pump. For monitoring the pressure a Penning (Pfeiffer Vacuum IKR 270) and a capacitive gauge (Pfeiffer Vacuum CMR 273) were used on the coating side of the system and the small chamber was equipped with an RGA (Thermo Scientific VGQ RGA MS) and a Penning gauge (Pfeiffer Vacuum IKR 270). The base pressure of the coating chamber was always within middle to low 10^{-8} mbar range and the base pressure of the small chamber was always in the middle 10^{-9} to middle 10^{-10} mbar range. The coating system is featured with three injection lines, one for Ar, one for H_2 and one for dry air which is used for venting.

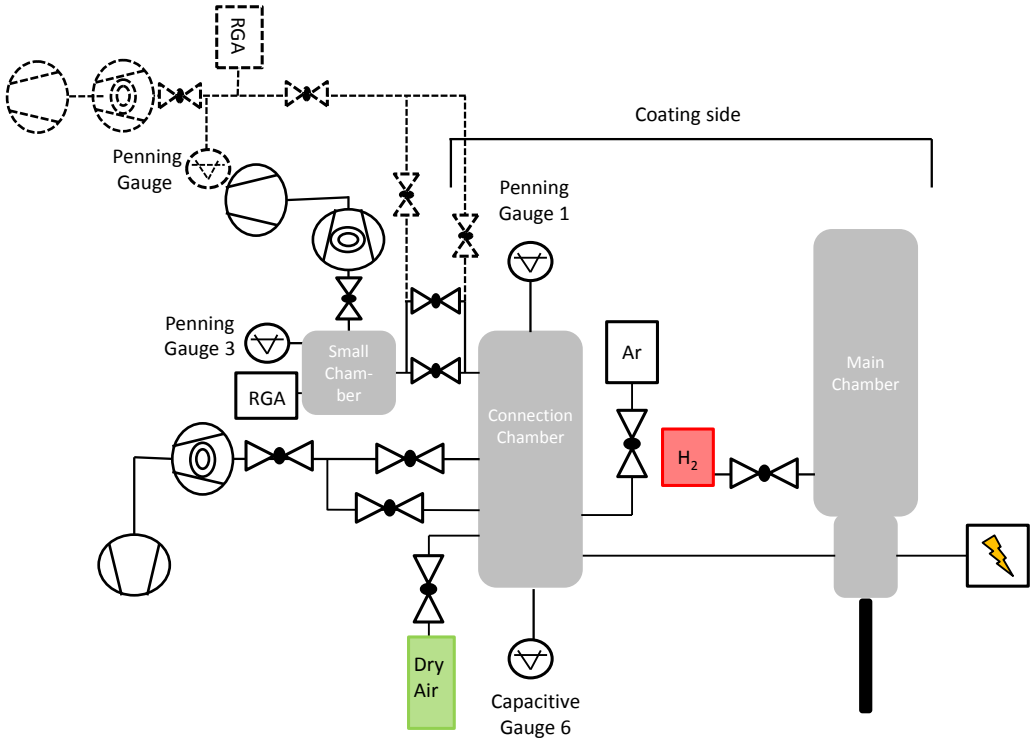

Figure 3.10: Schematic drawing of the coating system

During the experiments the sensitivity of the RGA from Thermo Scientific proved to be not sufficiently for a hydrogen concentration of less than 0.01 % in the working gas. Hence a mobile RGA system featured with an Pfeiffer QMG 700 RGA with higher sensitivity in a vacuum fired chamber was connected to the vacuum system. The mobile RGA set up with its own pumping group is illustrated in fig. 3.10 with dotted lines. The mobile RGA system is able to reach a pressure in the middle to low 10^{-10} mbar region.

Stainless steel liners, as shown in fig. 3.11, with openings for sample plates were used as substrate. In order to measure the thickness of the coating with a profilometer, an additional Si substrate was mounted on one of the afore mentioned openings. Pure graphite was used as target material in a specially developed hollow cathode configuration, shown in fig. 3.12.

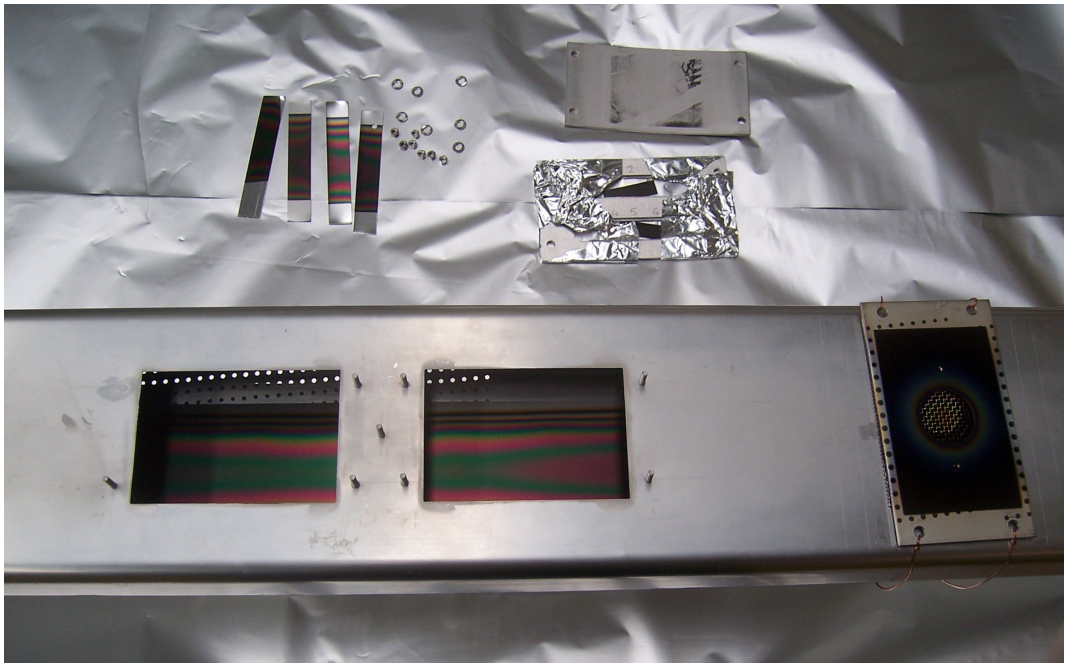

Figure 3.11: The image shows one of the liners and samples used as substrate after coating

Using a differentially pumped connection line between the coating side and the small chamber/mobile RGA made it possible to monitor the gas composition of the working gas in channeltron mode during the coatings even though a pressure of 1.15×10^{-1} mbar on the coating side was used. During the coating process the coating chamber was connected to the main pumping group only via a by-pass line with lower conductance in order to reduce the pumping speed. The correlation between the current reading of the RGA and the measured pressure by the Penning gauge for the desired hydrogen partial pressure was determined directly before every coating with full pumping speed in order to keep the contribution of the residual gas to a minimum. A correction factor of 2.4 for the H-pressure reading of the Penning gauge was taken into account. Furthermore the effect of the Ar injection on the H-pressure reading of the RGA was investigated.

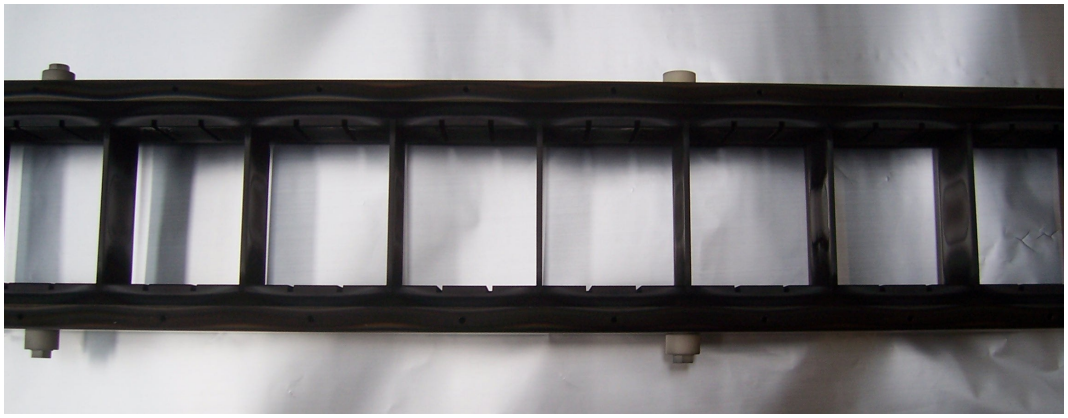

Figure 3.12: The image shows the used hollow cathode

Before and after every coating a scan of the residual gas of the small chamber and of the whole system were made. During the preparation of the coatings the H was always injected first. After the H pressure stabilised the Ar (gas bottle nominal purity 99.9999%) was added and after stabilisation the plasma was ignited. To avoid damages on the coating system due to quick thermal expansion of the cathode the power applied was ramped from 50 W to 200 W and then set to 120 W for the actual coating process. A Hüttinger PFG 1500DC DC generator was used as DC-power supply. To achieve a more uniform coating the cathode was connected to a motor that moved it back and forth. At the beginning of every coating the H pressure decreased due to the H implantation into the coating and the cathode. After stabilisation the H pressure was readjusted to the initial value. The whole coating process was always monitored by the RGA and an optical spectrometer. The Penning gauges had to be turned off during the coating, since the pressure on the coating side was too high for the Penning gauge and the Penning gauge of the small chamber/mobile RGA adulterated the RGA measurement due to ion-stimulated desorption. The substrate temperature varied freely during the coating process, no additional heating was applied.

After the coating the system always had time to cool down for 24 h. To exchange the liner and the samples the front part of the coating chamber had to be dismounted. The SEY and XPS measurements of the samples were carried out within 7 days after extraction.

3.3 SEY/XPS System

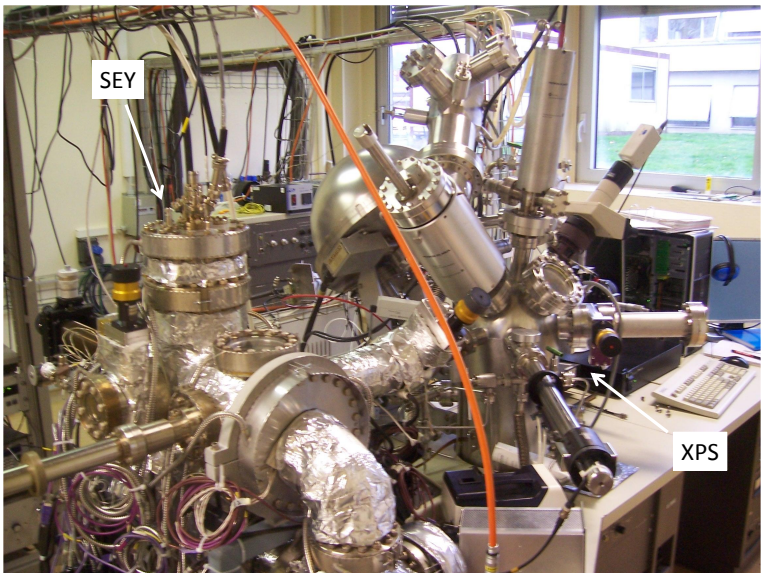

Figure 3.13: Image of the SEY/XPS system.

The SEY and XPS measurements were both carried out in the same vacuum system (fig. 3.13) that consists of two chambers, the chamber for the SEY measurements and a multi-purpose chamber. The samples can be transferred between the two chambers without air exposure. The multi-purpose chamber is equipped with an X-ray source, an ion gun, a quadrupole mass analyser that can be used together with the ion gun for SIMS and one Hemispherical Energy Analyser (HEA). The SEY chamber houses an electron gun, a flood gun, the electron collector and a modified manipulator. The set up is schematically shown in fig. 3.14. Both chambers have their own pumping groups consisting of an ion pump, a sublimation pump, a turbomolecular pump and a rotary vane pump. The SEY chamber features a Penning gauge for pressure measurement and the multi-purpose chamber is equipped with a Bayard Albert and a Penning gauge; both chambers house an RGA. The pressure in both chambers is normally within the high 10^{-10} mbar to high 10^{-9} mbar range.

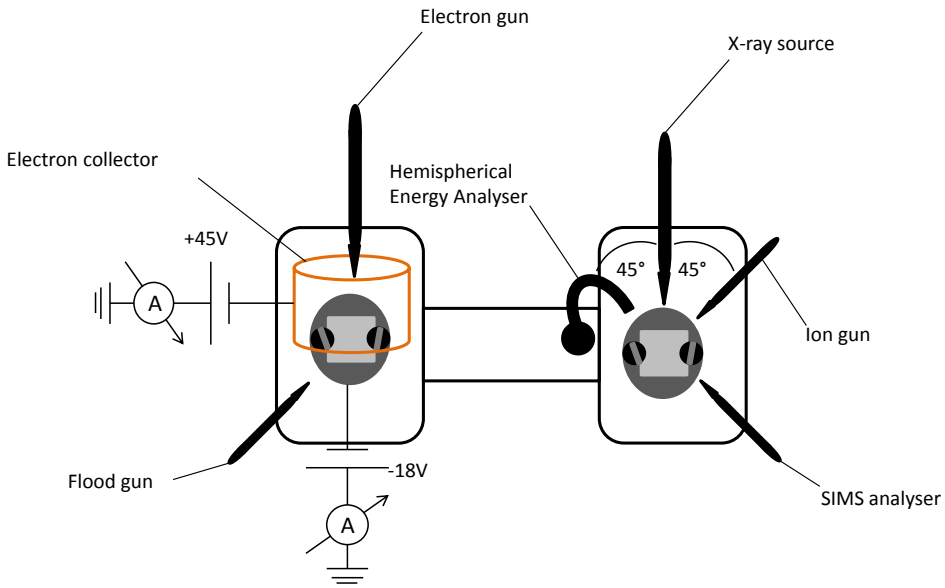

Figure 3.14: Schematic drawing of the SEY/XPS system

The SEY data were acquired using an electron gun normal to the sample's surface. The electron gun emits primary electrons within an energy range of 2 - 2000 eV. The primary electron energy was ramped in 50 eV steps from 32 - 1732 eV. The sample is surrounded by a positively (+45 V) biased electron collector for the detection of the secondary electrons. The sample was put on -18 V bias to guarantee that all secondary electrons are able to reach the collector. In this configuration the total SEY instead of the yield of the true secondary electrons (electrons emitted with an kinetic energy below 50 eV) was measured. An accuracy of $\pm$ 0.03 can be achieved in this way.

For the XPS measurements a non-monochromatized MgKα source (ESCA 5400) was used. The HEA (PHI model 10-360) looked at the sample in a 45° angle relative to the samples normal and was operated in Constant Analyser Energy (CAE) mode. From the XPS spectra the relative surface composition was determined by comparison of the peak area intensities after subtraction of a Shirley background.

4 Results & Discussion

4.1 Results Coating System

In order to produce carbon coatings with different SEY the general dependence of the SEY_{max} on the amount of hydrogen in the working gas was investigated. Fig. 4.1 shows this experimentally determined dependence. The SEY_{max} of amorphous carbon coatings shows a strong increase from 0.94 without hydrogen injection to 1.48 at a ratio H_2/Ar of 0.09 %. Above 0.09 % hydrogen of the working gas pressure only a slow increase of the SEY_{max} is observed. The reason why the amount of hydrogen in the working gas affects the SEY of the carbon coating has not been understood yet, but a possible explanation would be that the hydrogen reacts with the carbon and stabilises preferentially sp^3 hybridization. The complete SEY and XPS results are given by tab. 4.1. The traces of argon found in the coating without hydrogen injection are related to ions neutralised by inelastical scattering by the cathode which are implanted into the coating. For the coating without hydrogen injection a hydrogen partial pressure of 1.76×10^{-6} mbar was extrapolated using a linear fit of two measurements with hydrogen injection, the RGA reading of the coating without hydrogen was then correlated to the corresponding partial pressure on the fitted curve. This partial pressure would correspond to a hydrogen concentration in the working gas of 0.0037 %. The extrapolated value however is strongly affected by the ion induced desorption in the RGA itself caused by the high argon pressure and mainly represents an upper limit for the amount of hydrogen during the coating.

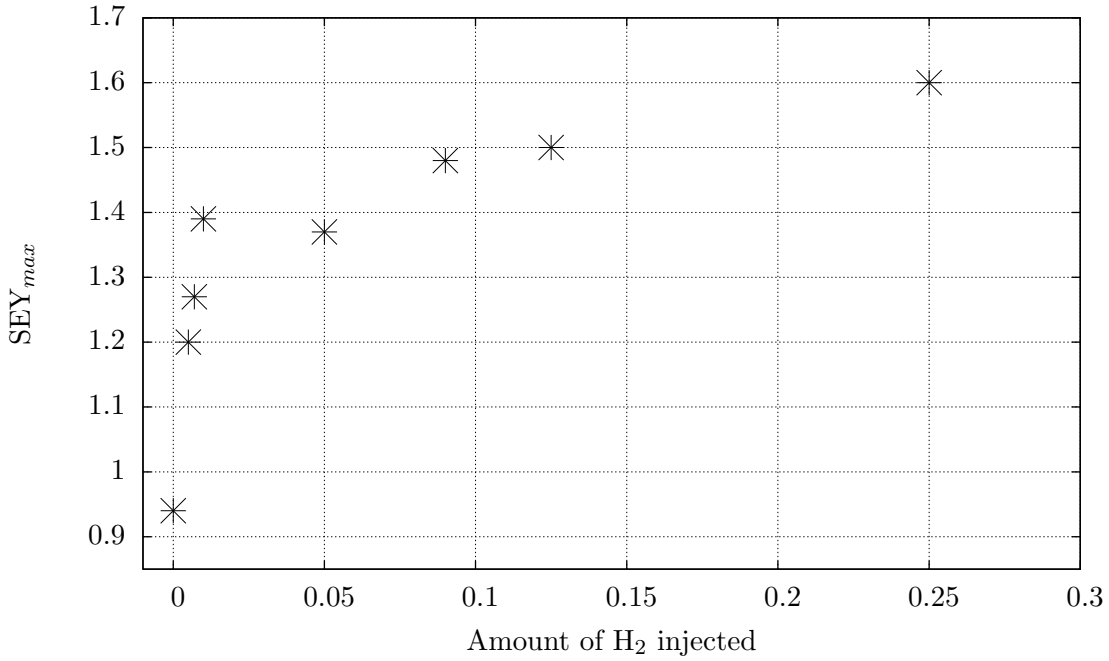

Figure 4.1: Dependence of the SEY$_{max}$ on the amount of hydrogen in the working gas.

Table 4.1: XPS and SEY results of the carbon coatings produced under hydrogen injection.

H_2/Ar [%]	C [At%]	O [At%]	Ar [At%]	SEY$_{max}$
0	88.8	10.9	0.3	0.94
0.005	91.2	8.8	-	1.20
0.007	93.0	7.0	-	1.27
0.01	91.6	8.4	-	1.39
0.05	94.2	5.8	-	1.56
0.09	93.5	6.5	-	1.48
0.125	92.8	7.2	-	1.5
0.25	92.6	7.4	-	1.6

The XPS measurements show that the amount of hydrogen in the working gas affects the shape of the C1s line, this favours the hypothesis that the hydrogen changes the chemical state of the carbon. Fig. 4.2 shows this dependence. The C1s lines of the coatings with a low amount of hydrogen and a low SEY show a slower decrease on the higher binding energy side than the coatings with a higher hydrogen partial pressure. This correlation is represented by the right part of fig. 4.2.

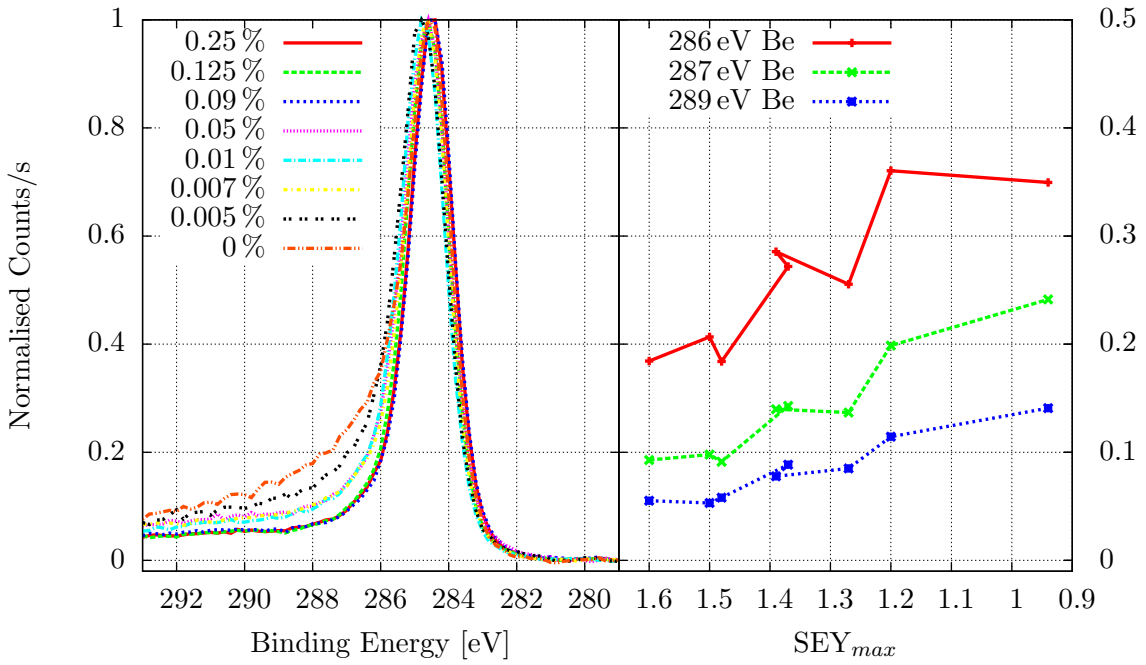

Figure 4.2: Normalized C1s lines of the carbon coatings with different hydrogen concentration left and the intensity of the C1s line for 286 eV, 287 eV and 289 eV right.

4.2 Results Multipacting Test Bench

4.2.1 General Observations

As already observed during previous work [4] the intensity of the current and the pressure rise during Multipacting shows an exponential decay, which is at the beginning dominated by the SEY decrease due to the electron stimulated desorption and later by the carbonaceous film growth. Due to the decreasing SEY an increase in the threshold power to excite Multipacting is observed in the current, the pressure increase and the change in reflected power. Furthermore, as shown in fig. 4.3 intensified Multipacting occurs if the cyclotron resonance frequency of the applied magnetic field approaches the frequency of the RF signal.

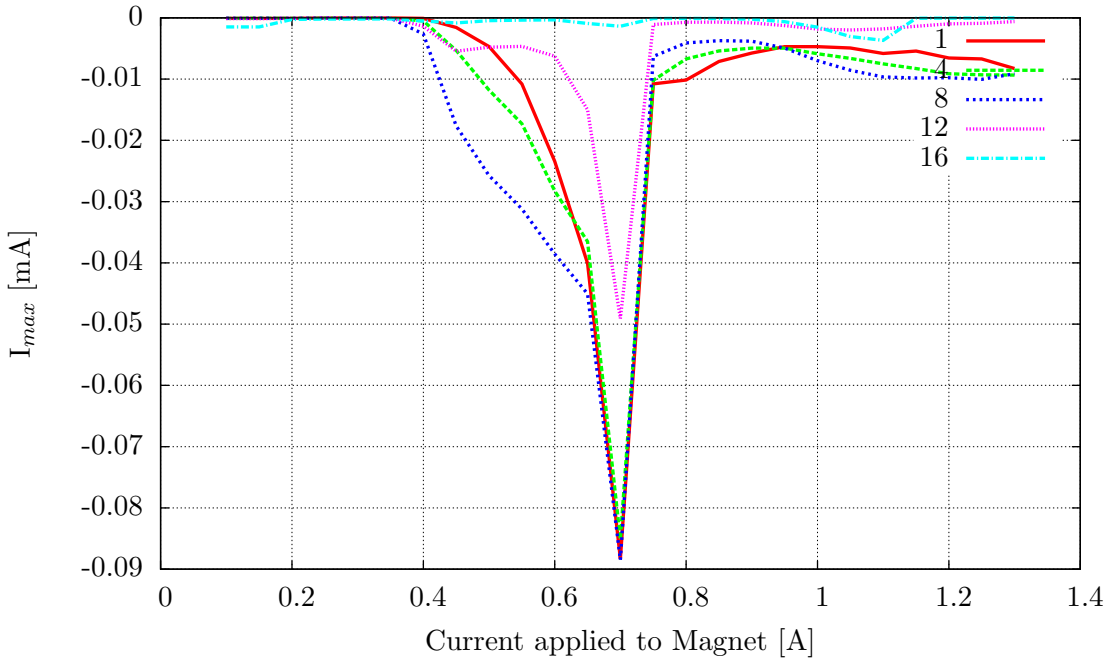

Figure 4.3: Maximum current as a function of the current applied to the magnet for the channels 1, 4, 8, 12, 16 of the transversal stripe detector.

Fig. 4.4 shows the correlation between the carbon detected on the surface and the SEY_{max}. The black circles mark the reference samples and the blue circles mark the samples related with a test regarding the effect of the vacuum system itself. The SEY dependence shows two trends, an increase of the SEY with the amount of carbon in case of the reference samples and a decrease in case of the samples exposed to the electron cloud. The reference samples accumulated carbon on their surfaces due to carbonaceous adsorbates accumulated as a result of the poor vacuum. This was also confirmed by the vacuum test during which the SEY and XPS of a sample were measured directly before and after introducing it into the vacuum system for one week without initiating any Multipacting. The test showed an increase in the amount of carbon from 26.4 to 45.9 At% and an increase in the SEY from 1.96 to 2.28. The samples exposed to the electron cloud also accumulate carbon on their surface, but due to the energy transferred by the striking electrons a different ratio between sp^2 and sp^3 hybridization with a comparable low SEY is achieved. The measurement point marked with the red circle is the only measurement which does not fit the behaviour of the other conditioned samples.

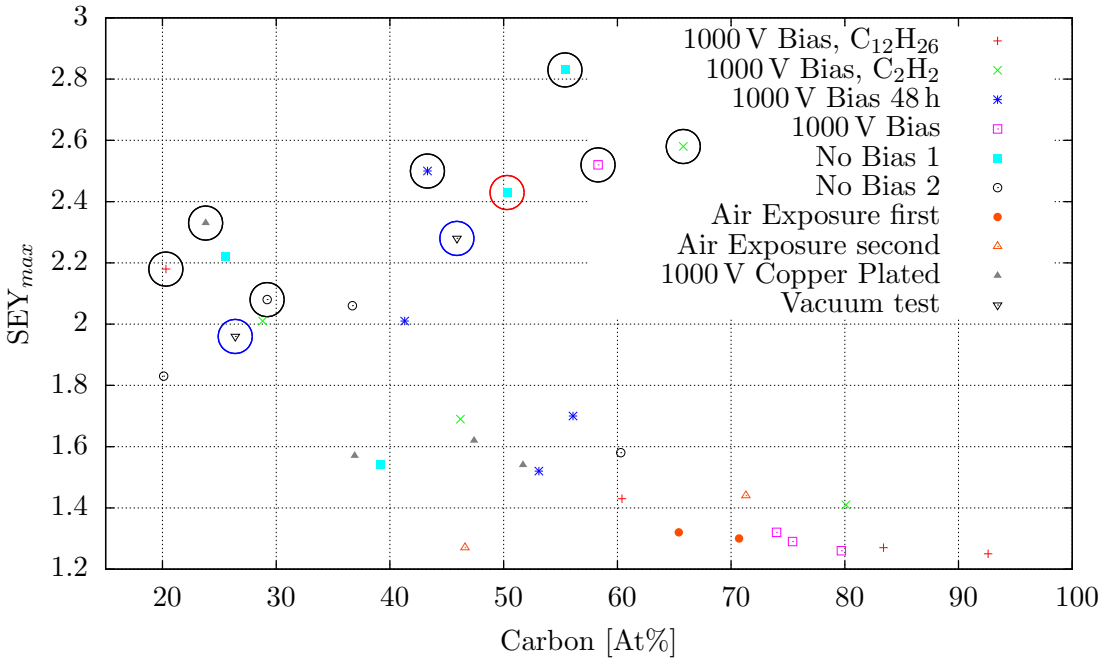

Figure 4.4: SEY as a function of the carbon present on the surface, the black circles mark the reference samples.

The correlation between the SEY$_{max}$ and the cumulative dose is represented in fig. 4.5. A fast decrease of the SEY with the cumulative dose was observed, this fits also very well to results from older experiments performed on the SEY system with the flood gun. The SEY results show a large scattering between a cumulative dose of 10^{-4} and a cumulative dose in the low 10^{-3} C/mm^2 range. A possible explanation for this behaviour might be a dependence of the memory effect of the conditioning after air exposure on the thickness of the accumulated carbon layer.

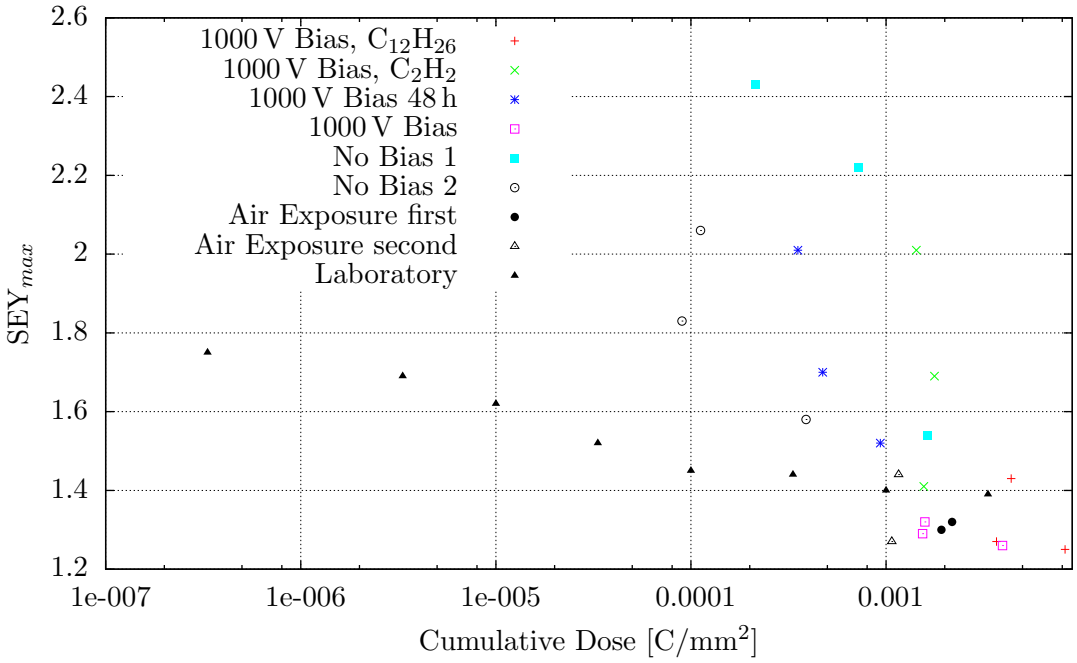

Figure 4.5: SEY as a function of the cumulative dose averaged over the width of the liner, the x axis is given in logarithmic scale.

4.2.2 The effect of a DC Bias Voltage on the Multipacting

Previous work [4] showed that using only the electric field caused by the RF signal is not sufficient to reach an SEY of 1.3 through surface conditioning. Hence, an interest in increasing the electron energy arose. In order to give the electrons more energy a DC bias voltage was applied to the tungsten wire. The experiments showed, that it is not possible to develop Multipacting by using a negative bias voltage of -100 V or more, but as shown in fig. 4.6 the maximum current shows a nearly linear correlation with a positive bias voltage up to 1000 V. It was not possible to apply voltages above 1000 V since this is the maximum voltage the DC blocks used in the present study are able to withstand.

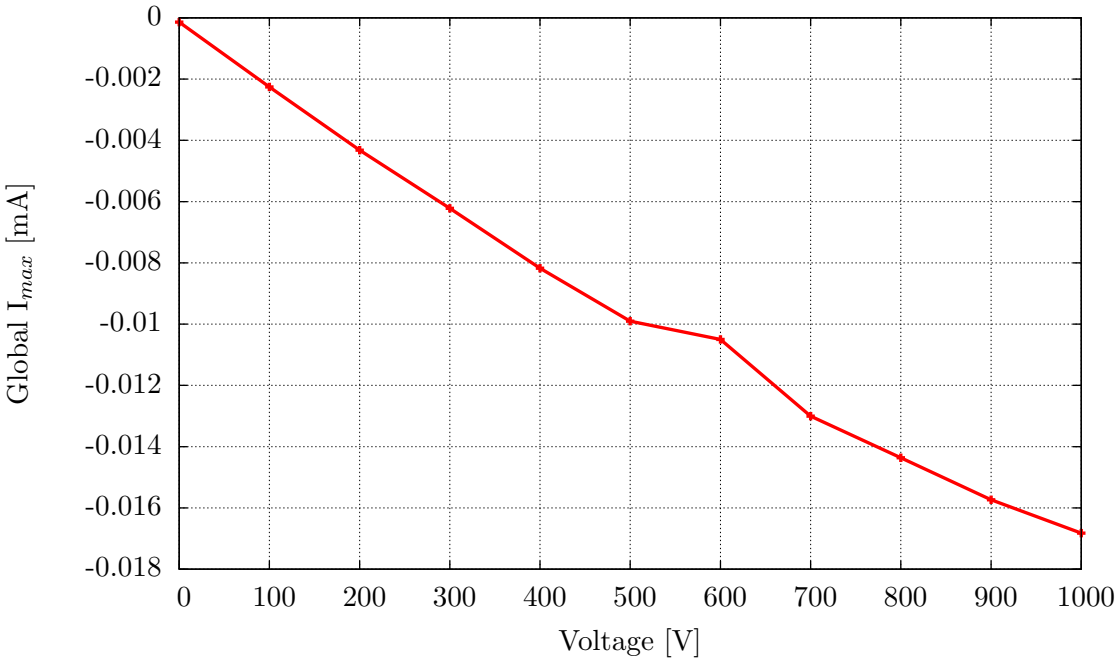

Figure 4.6: Global maximum current as a function of the DC bias voltage measured in the end of a run with 1000 V Bias, acquired with the longitudinal stripe detector.

An explanation for suppressing the Multipacting with the negative bias voltage might be that the secondary electrons emitted are reflected by the negative potential on the wire and therefore are not able to cross the chamber and to gain enough energy to produce secondary electrons themselves. Why the positive bias voltage on the other hand does not function as a clearing electrode has not been fully understood yet. The increase of the maximum current with the voltage, shown in fig 4.6, might be an indication that the initial electron energy was below the energy of SEY_{max}.

A measurement run started without bias voltage was carried out during which a DC Bias Voltage of +400 V was applied after 4764 shots. The bias voltage led to an immediate increase of the global maximum current from -0.024 mA to -0.037 mA. This enhancement of the Multipacting accelerated the conditioning and therefore decreased the global maximum current below the value measured without bias voltage within 30 shots. The decay of the global maximum current during the Multipacting run is represented in fig. 4.7.

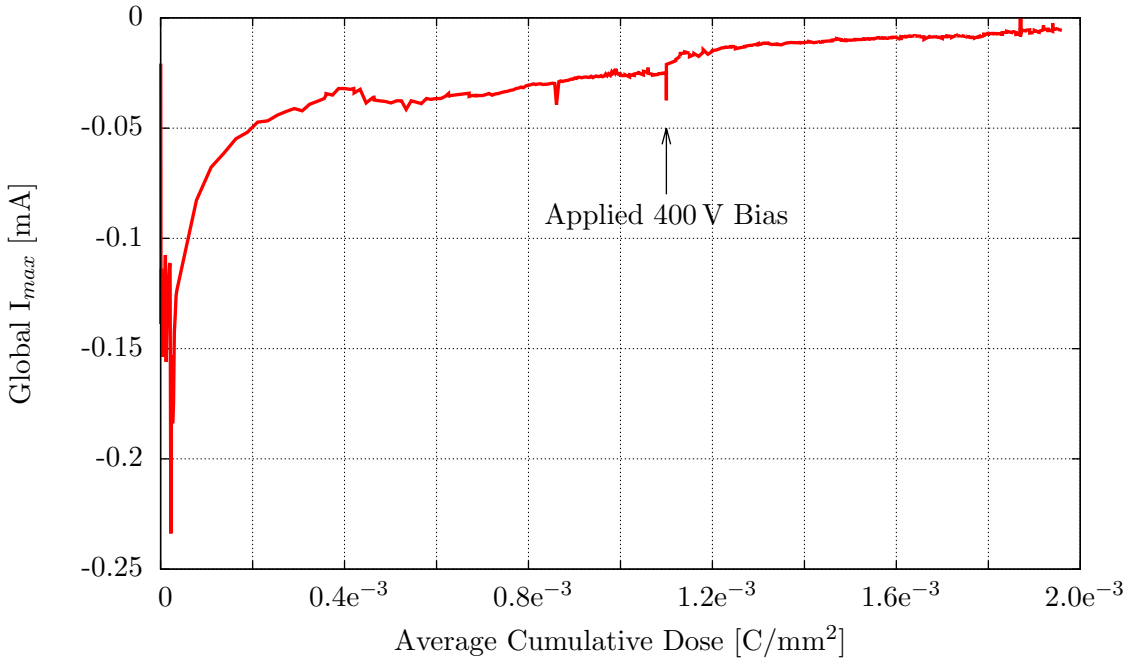

Figure 4.7: Development of the maximum current during the Multipacting run with a DC bias voltage of +400 V applied after shot 4764, acquired with the longitudinal stripe detector.

Multipacting runs without and with a bias Voltage of +1000 V were carried out for direct comparison. As shown in fig. 4.8 the average cumulative dose (CD) increased much faster with bias voltage than without and reached 2.85×10^{-3} C/mm^2 with bias voltage compared to only 6.34×10^{-4} C/mm^2 without bias voltage after 11 days of conditioning. Thus the average cumulative dose accumulated with a DC bias voltage of +1000 V equals approximately five times the average cumulative dose of a measurement run without bias voltage.

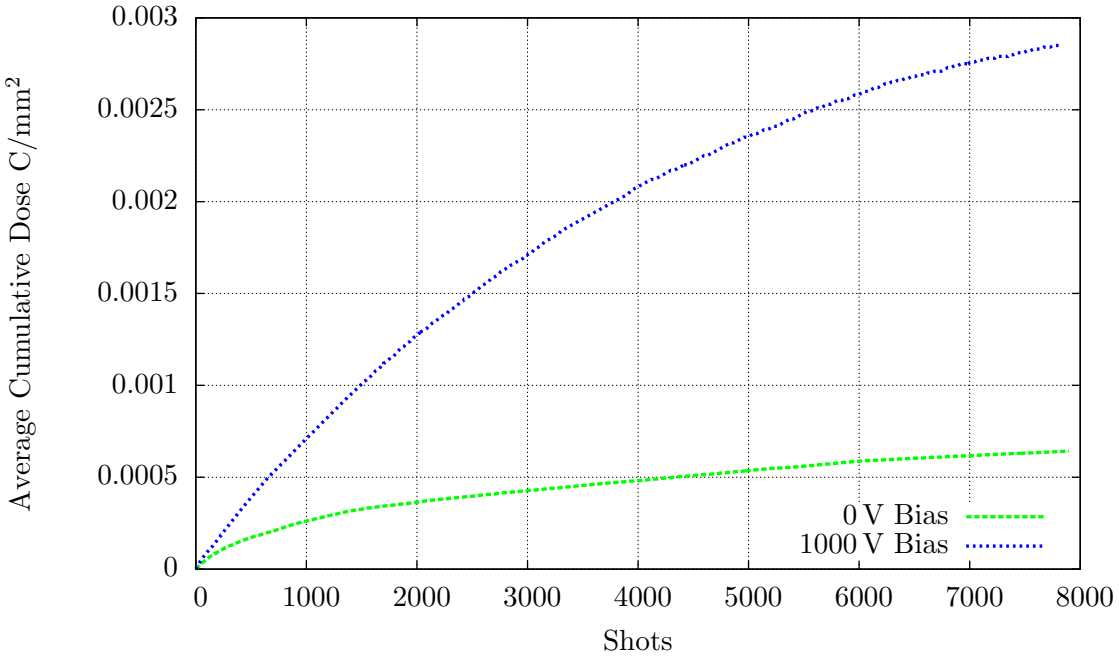

Figure 4.8: Cumulative dose during a Multipacting run with +1000 V DC bias voltage and without bias voltage, acquired with the longitudinal stripe detector.

This behaviour can also be observed by taking a look at the evolution of the global maximum current during the measurement run. For the same cumulative dose the global maximum current during a measurement run with a bias voltage is always higher than during a run without bias voltage. Fig. 4.9 compares two such runs. The sudden decreases at an average cumulative dose of 0.0005 C/mm^2 and 0.0007 C/mm^2 are not understood. Both measurement runs developed after some time a periodical variation in the maximum current, which might be due to a change in the position or the shape of the electron cloud. The spikes in the curve of current taken with bias voltage correspond to single shots manually applied without bias. These shots are used to compare the conditioning state of the surface to a measurement run without bias voltage for the same cumulative dose. These measurement points correlate at the beginning of the run very well with the measurement run without bias voltage. This shows that the resulting current depends only on the accumulated dose and therefore the limiting factor for the conditioning during previous work had been the accumulated dose and less the electron energy. Fig. 4.9 also shows that the surface conditioning after 5650 shots is advanced enough to completely suppress the electron cloud build up during shots applied without bias voltage.

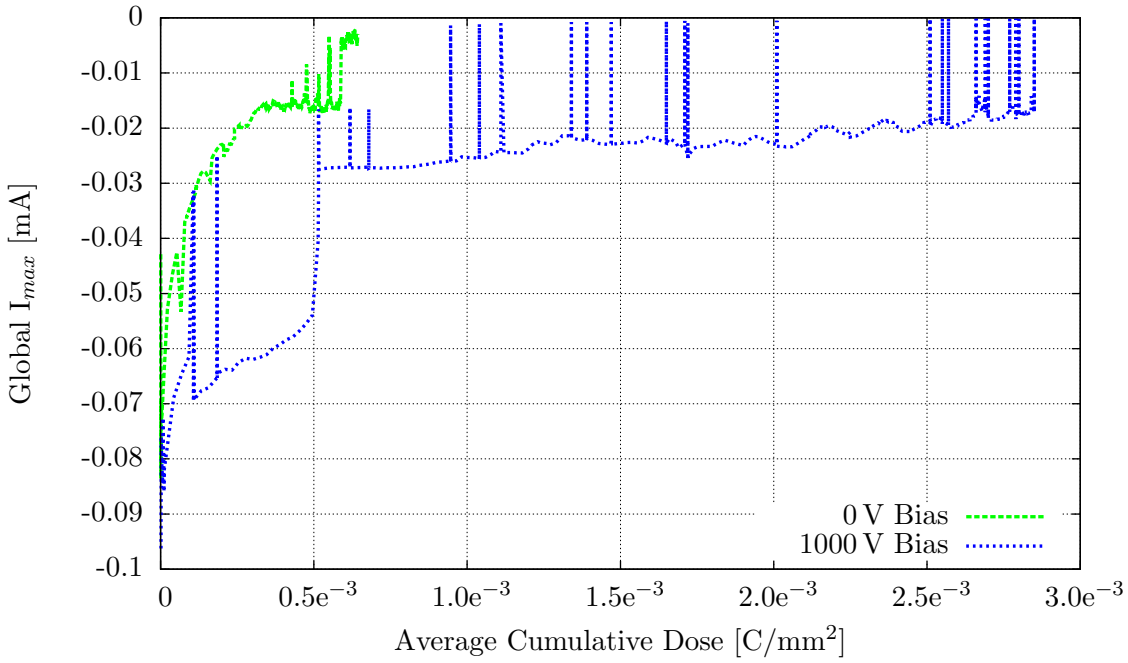

Figure 4.9: Development of the maximum current during the Multipacting run with a DC bias voltage of +1000 V and without bias Voltage, acquired with the longitudinal stripe detector.

The higher number of electrons impinging on the surface also enhances the electron stimulated desorption and therewith the pressure increase during the shots. As shown in fig. 4.10 the delta pressure with applied bias voltage stays constantly above the delta pressure achieved without bias voltage. Furthermore, it was observed that the decrease of electron induced outgassing progresses faster than the current decrease and therewith the limiting factor for the electron stimulated desorption becomes at some point the amount of adsorbates accumulated on the surface of the liner during the 90 s break in between two RF power ramps instead of the dose per shot. A similar behaviour had been already observed by Henrist et al. [15]. The sudden peaks in the maximum pressure for both measurements have not been fully understood yet, one possible explanation might be changes in the ambient temperature or a change in the position of the electron cloud smaller than the resolution of the stripe detector.

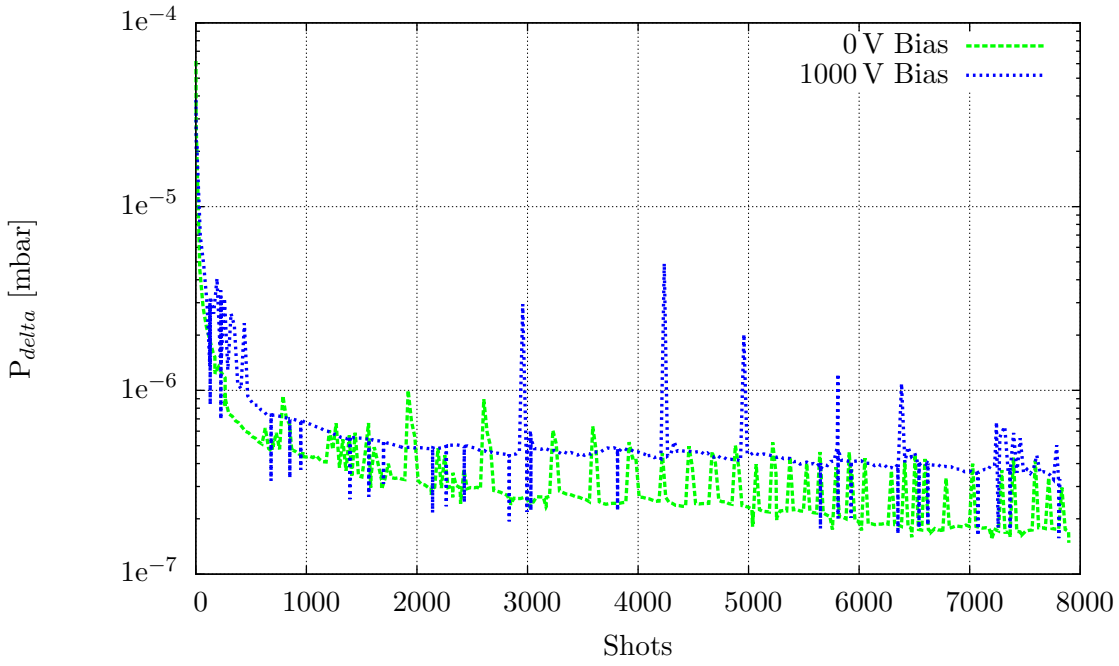

Figure 4.10: Pressure development during a Multipacting run with +1000 V DC bias voltage and without bias voltage.

For single shots during the measurement runs RGA spectra were acquired. Since the Multipacting lasts only for a few seconds it was not possible to measure the masses from 0 to 100 at once. Hence, fast RGA scans from 0-33, 34-67 and 68-100 were applied during three consecutive shots. One such RGA scan lasts 6.6 s compared to 8-9 s of pressure rise due to the Multipacting. The baseline was always measured directly before the shot, during the shot a series of scans was carried out, the scan with the highest pressure was chosen for data analysis. Since the pressure varies during the RGA scan the results are not very accurate. The data of the three scans were afterwards merged. Such RGA spectra of three shots with 1000 V Bias and without bias voltage before and during the Multipacting are represented by fig. 4.11. All RGA spectra were normalised respectively to atomic hydrogen and the baseline was subtracted in order to make it possible to compare RGA spectra from different runs at different base pressures. The atomic hydrogen was chosen as a reference for the normalisation since it remains stable during the Multipacting and is mainly produced by the RGA itself.

The spectra of both runs show a lot of oxygen (16,32) and Nitrogen (14,28), these are signs of a small leak. Both spectra show an increase of mass 28 and 2 during the Multipacting, which is mainly related with the high cross section of carbonmonoxide and

hydrogen for electron stimulated desorption. In the case of the run with bias voltage a much stronger increase in the molecular hydrogen (2) and carbondioxide (44) due to the higher dose per shot was observed, furthermore during the Multipacting masses related with Hydrocarbons between 37 and 43 appeared.

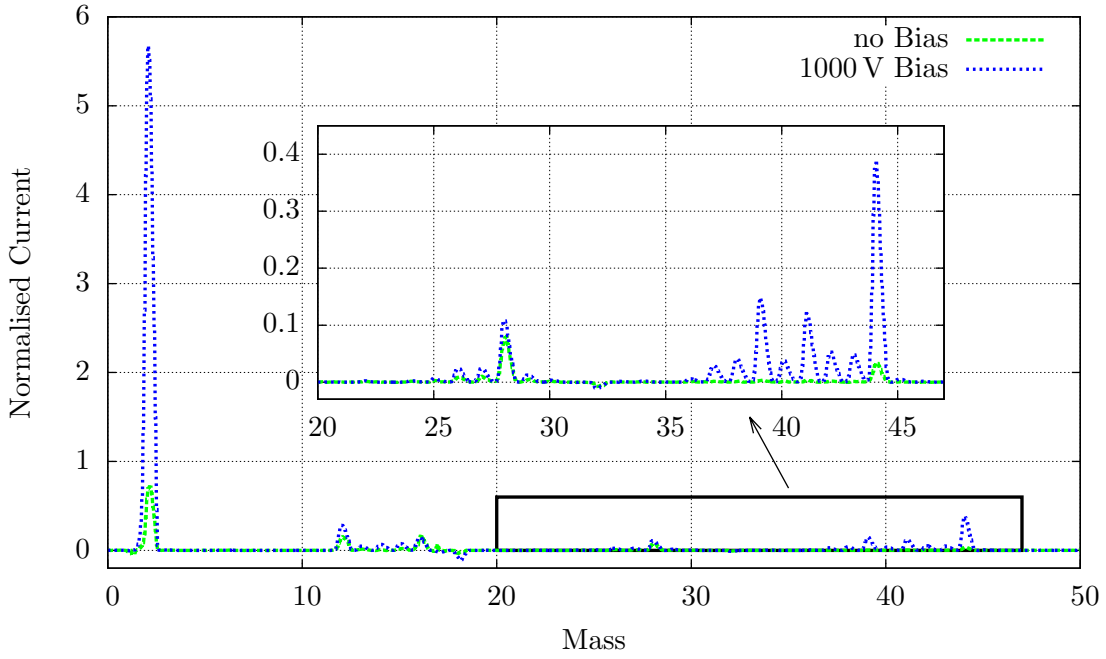

Figure 4.11: Normalised RGA scan with a SEM voltage of 1200 V of a shot with and without bias before and during Multipacting.

The SEY and XPS results performed directly after taking the samples out of the Multipacting test bench are in very good agreement with the Multipacting behaviour during the measurement run. The SEY/XPS results are given by table 4.2. As reference 1 the unconditioned back side of the sample was used and reference 2 corresponds to a sample stripe that was measured directly after chemical cleaning and had never seen the Multipacting test bench. The two references were used in order to see the effect of the vacuum system on the samples.

The XPS results showed that the samples accumulated carbon on their surface due to the surface conditioning. The very similar carbon concentration of the sample conditioned without bias voltage and with 1000 V bias voltage might be an indication that the quantity of carbon accumulated on the surface was not the limiting factor for the reached SEY. Therefore, the main factor might be the kind of carbon. The additional dose might have changed the ratio between carbon with sp^2 and sp^3 hybridization.

Table 4.2: XPS and SEY results of the measurements with and without bias voltage, CD in the first column from the right stands for cumulative dose.

Sample	C [At%]	Cr [At%]	F [At%]	Fe [At%]	N [At%]	O [At%]	SEY_{max}	CD [C/mm^2]
0 V Bias	64.3	4.2	1.3	3.0	1.4	25.7	2.23	1.64 e^{-3}
400 V Bias	78.2	2.7	0.9	1.2	2.2	15.0	1.52	1.96 e^{-3}
1000 V Bias	64.1	3.3	1.6	3.5	2.9	24.6	1.33	6.14 e^{-3}
Reference 1	45.6	4.9	1.6	4.8	2.1	29.1	2.50	-
Reference 2	11.9	13.9	-	11.0	1.4	56.0	1.87	-

By comparing the shape and position of the C1s line information about the chemical state of the carbon can be gained. Therefore fig. 4.12 represents the normalised C1s lines of the sample with 0 V Bias, with 1000 V bias and the two reference samples. In the case of the two reference samples an additional feature at 288.5 eV binding energy can be observed which generally corresponds to C=O bonds. For reference 2 another feature at 286 eV binding energy was present, this might be related with C-OH bonds present on the surface [25]. These features are missing in case of the two conditioned samples, since the C=O and the C-OH bonds have been removed by the electron stimulated desorption during the conditioning. The sample from the Multipacting run with 1000 V bias voltage shows a slower decay on the high binding energy side than the sample from the Multipacting run without bias voltage. Furthermore a shift to lower binding energies can be observed in the case of the sample conditioned with bias voltage. This might be an indication for a higher concentration of graphitic carbon in the sample conditioned with +1000 V bias voltage [9].

The SEY results showed that by applying a bias voltage it is possible to accelerate the conditioning process. Therefore, it was possible to reach an SEY of 1.33 after 11 days with 1000 V bias compared to an SEY of 2.23 without bias voltage. The SEY results are also represented in fig. 4.13.

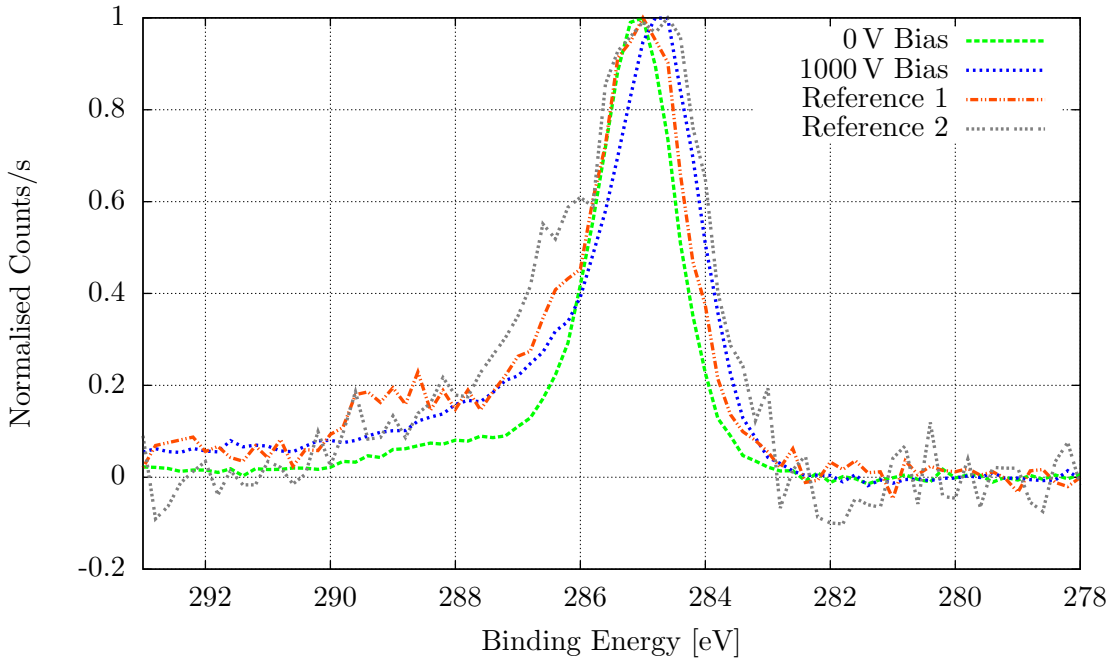

Figure 4.12: The normalised C1s lines of the measurements with and without bias voltage.

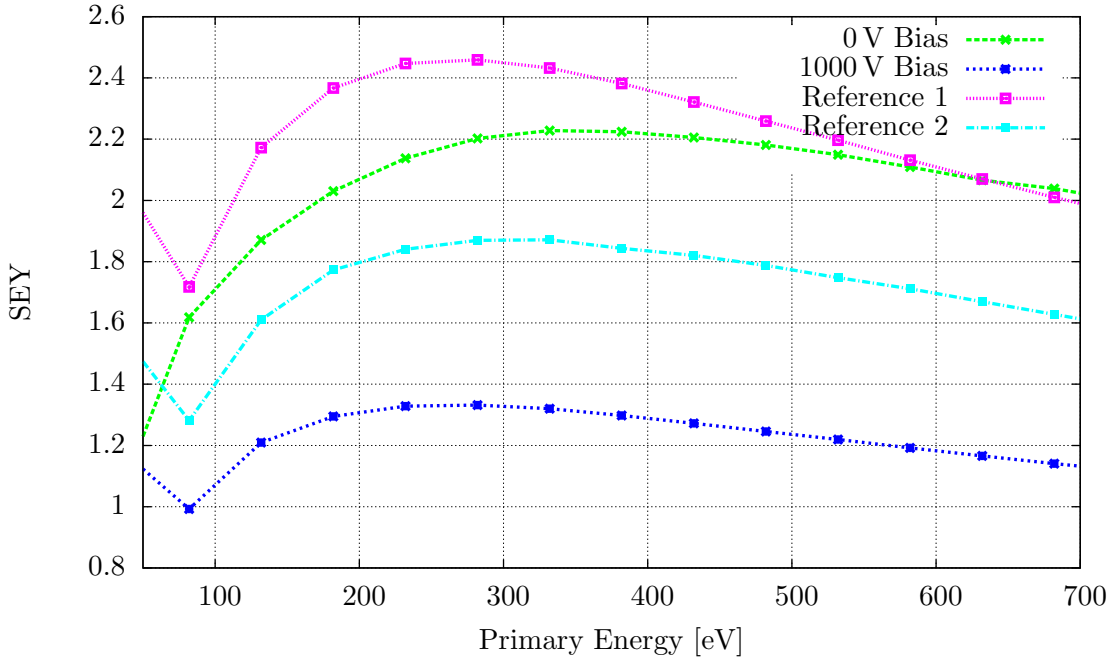

Figure 4.13: The measured SEY curves with and without bias voltage.

4.2.3 Electron cloud distribution inside the liner

In order to get a better understanding of the e-cloud build up and behaviour the e-cloud distribution along the length and width of the liner was measured during conditioning with and without bias voltage.

Transversal e-cloud distribution

As shown in fig. 4.14 left for measurement runs without bias voltage only minor changes in the electron distribution over the width of the liner were observed as a function of the number of shots applied. The maximum of the e-cloud showed a decrease during conditioning and was located in the middle of the liner during the whole run.

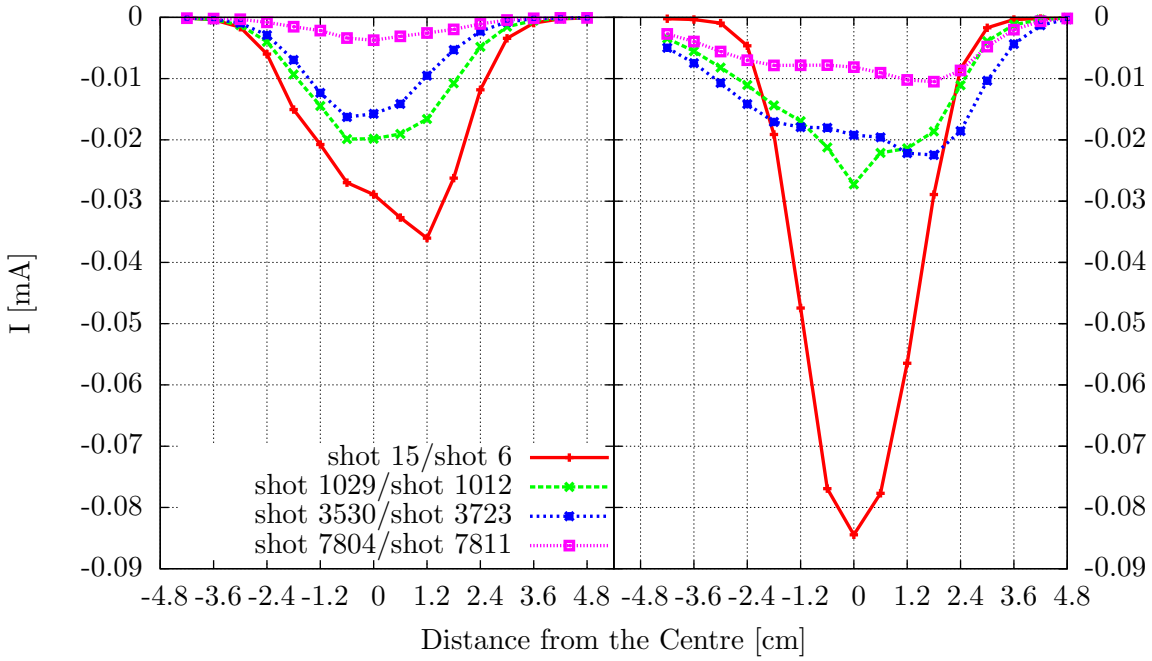

Figure 4.14: Development of the transversal electron cloud distribution during a measurement run without bias voltage (left) and a measurement run with 1000 V bias voltage (right).

However, for the measurement run with a bias voltage of 1000 V a clear change in the e-cloud distribution during conditioning was observed (fig. 4.14 right). The maximum decreased during the Multipacting run and changed from a single maximum at the centre to two separate maxima at about 1.8 cm from each side of the central channel. This shift can be explained by the progress in the conditioning of the liner surface: due to the higher dose in the centre of the liner during the beginning of the measurement the

centre conditions faster and therefore the SEY in the centre decreases below the SEY on the sides. For the Multipacting run without bias voltage the SEY increased going from the centre to the side from 2.23 to 2.37 and for the run with a bias voltage of 1000 V the SEY increased from 1.33 to 1.71 (SEY values measured at the end of the run after air exposure).

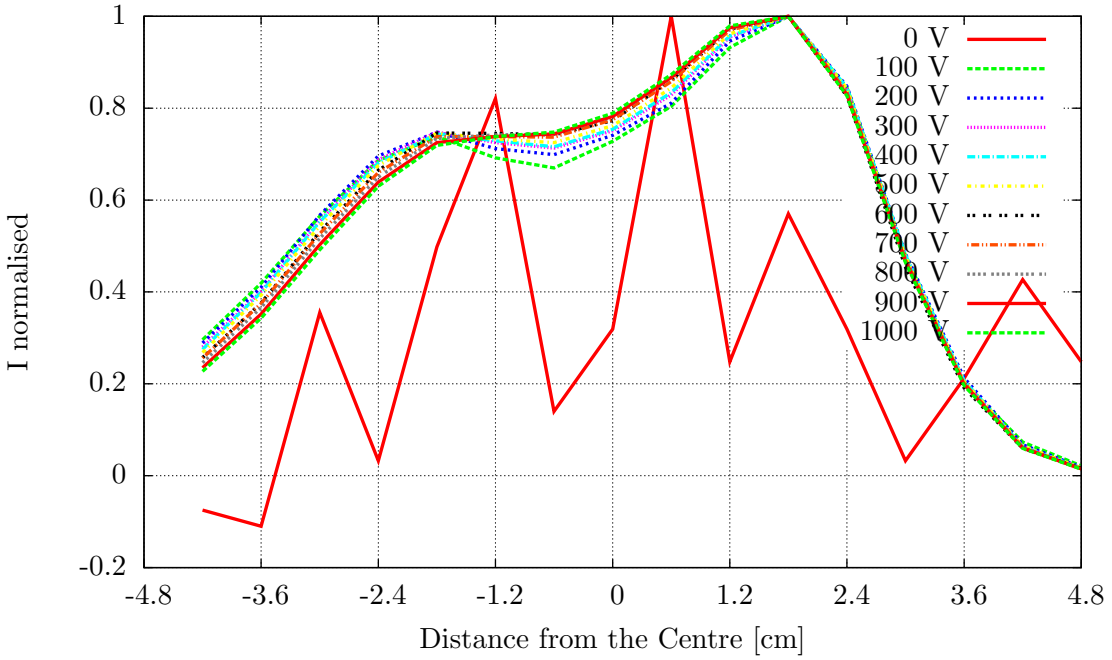

Figure 4.15: Normalised transversal electron distribution in dependence of a bias voltage, measured after 11 days of conditioning with a bias voltage of 1000 V.

Fig. 4.15 shows ten shots applied with different voltages carried out at the end of a Multipacting run with 1000 V bias. For the case without bias no Multipacting was observed since the conditioning of the surface was already too advanced. However as soon as a positive bias voltage was applied Multipacting was stimulated. Anyhow, the electron distribution along the width of the liner did not show any dependence on the applied DC bias voltage.

Longitudinal e-cloud distribution

Previous measurements raised doubt about the homogeneity of the electron cloud along the length of the liner. Hence, a transversal stripe detector was used to study the Multipacting behaviour along the length of the liner. As shown in fig. 4.16 without

bias voltage and with a bias voltage of 1000 V the Multipacting was at the beginning of the run concentrated on the first couple of centimetres of the liner (the front of the liner is in the following defined as the side closer to the matching) and moved slowly towards the middle during the run. This movement of the electron cloud was caused by the progression of the surface conditioning.

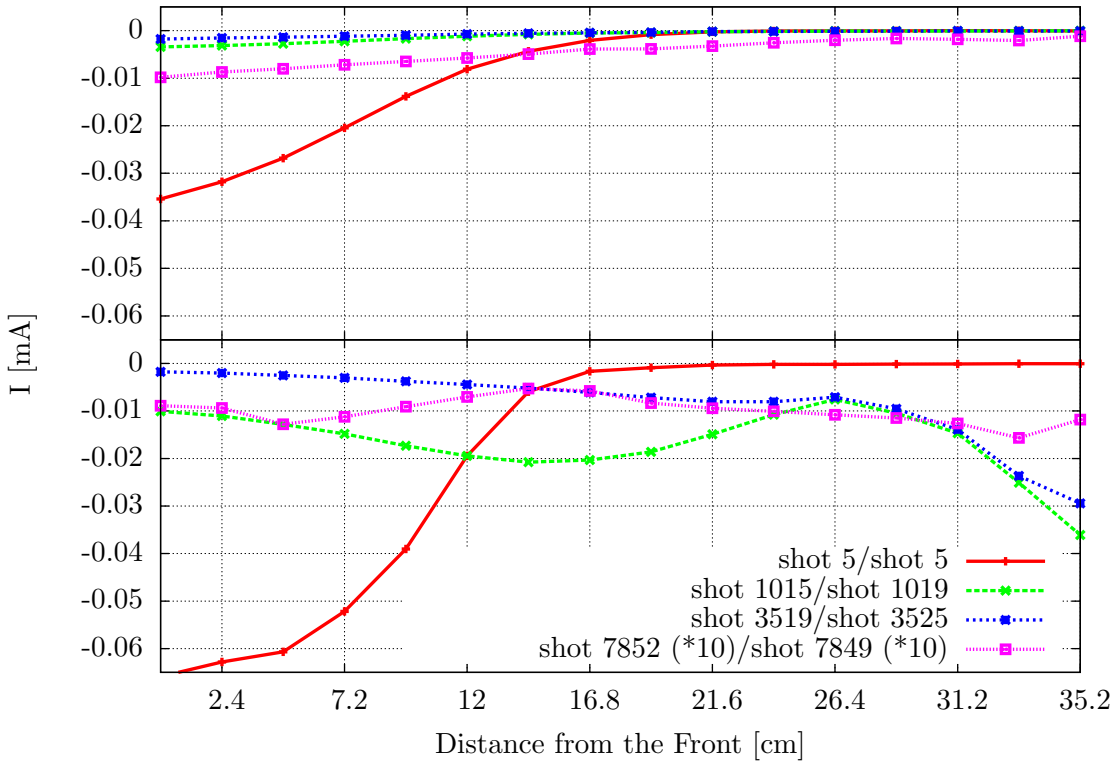

Figure 4.16: Development of the longitudinal electron cloud distribution during a measurement run without bias voltage (top) and with a bias voltage of +1000 V (bottom).

During the run both cases showed the development of an additional Multipacting feature at lower threshold power in the rear of the liner, represented in fig. 4.17. This feature initially has a higher threshold power than the Multipacting in the front of the liner. Since the Multipacting in the front of the liner consumes a part of the RF power injected into the resonator the threshold power to ignite the Multipacting in the rear is not reached during the power ramp. During the measurement runs the threshold power for the Multipacting in the front increases due to the progression in the surface conditioning and therefore the value for threshold power in the front approaches

the threshold value for the rear at some point. However, this additional Multipacting feature was much stronger developed during the runs with bias voltage. The reason for the stronger appearance of this feature during the runs with bias voltage is the higher conditioning speed in the front of the liner due to the faster accumulation of electron dose. During the runs this feature moved to higher threshold power and became in the runs with bias voltage at some point dominating over the Multipacting in the front and middle of the liner. This feature also led to a strong difference in the SEY in the rear of the liner between the runs with (SEY 1.26) and without bias voltage (SEY 1.43).

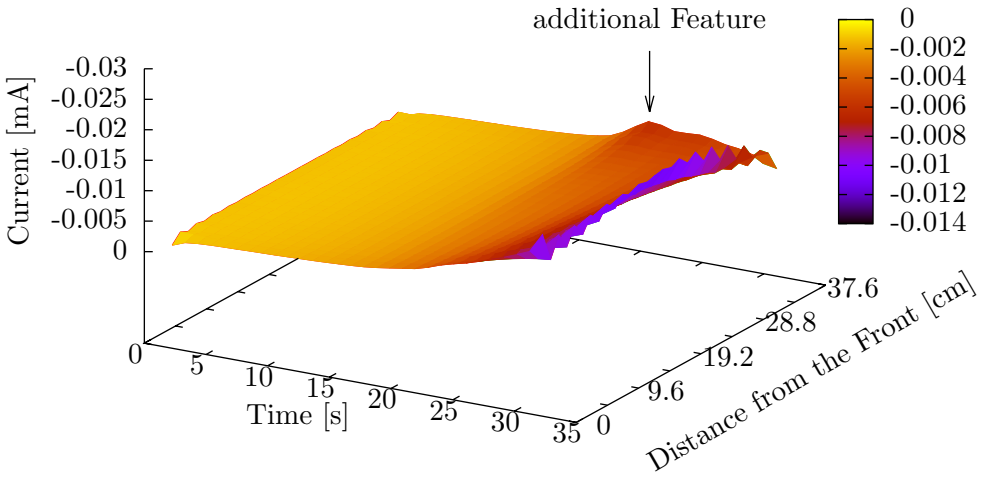

Figure 4.17: Current during one shot with bias voltage of 1000 V over all channels

4.2.4 Reconditioning after air exposure

Since the accelerators are vented from time to time for maintenance and improvements a measurement run with air exposure was carried out. The goal of this run was to see if the effect of the conditioning state obtained before the venting can be maintained or if this is not the case how long it takes to reach the same state as before the air exposure. To investigate this, one liner was conditioned for four days with applied bias voltage of 1000 V, exposed to air for one week and reconditioned for another four days. Samples corresponding to channel 1 and 8 from the stripe detector were measured after the two conditioning runs and after 19 days of storage on air wrapped in aluminium foil.

After exposing the liner to air the multipacting current increased, compared to the one at the end of the first conditioning, so that the received dose per shot increased by one order of magnitude up to 3.78 C/mm^2. However, this value is still lower than the one before any conditioning (3.84 C/mm^2), showing that some memory of the first conditioning was kept even after air exposure. Furthermore, as shown in fig. 4.18, the dose per shot during the second conditioning decreased much faster as a function of the number of cycles. This might be an indication that some of the carbon from the first conditioning remained and that the high dose per shot at the beginning of the second conditioning was mainly due to adsorbates accumulated during the air exposure.

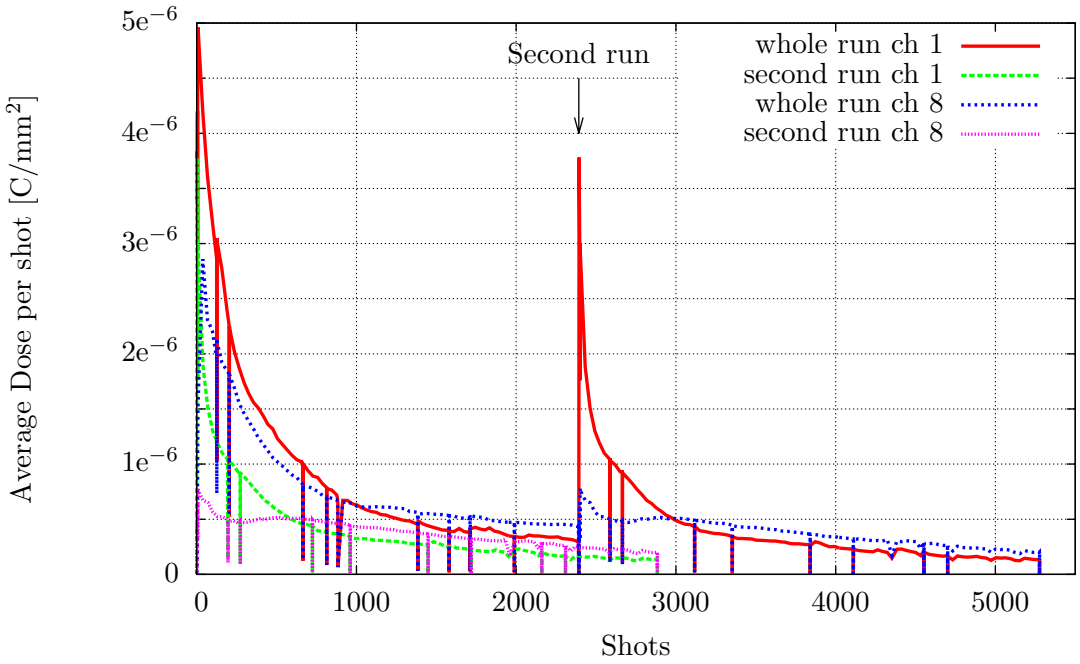

Figure 4.18: Dose over shots of channel 1 and 8 for the measurement run with air exposure, acquired with transversal stripe detector.

After the first conditioning an SEY of 1.32 at ch 1 and 1.3 at ch 8 was reached. The sample corresponding to channel 8 showed a decrease in the SEY of 0.03 after the second conditioning run even though the amount of carbon decreased by 18.8 At%. Whereas the sample corresponding to channel 1 showed an increase in the SEY of 0.12 with a similar amount of carbon present on the surface. The SEY/XPS results after 19 days of air exposure showed barely any change, the SEY of the sample corresponding to channel 1 stayed constant, the SEY of the sample corresponding to channel 8 increased by 0.07. Furthermore, no changes in the shape and position of the C1s line could be found. A

possible explanation for the small variation after the 19 days of air exposure might be that the surface saturates within the first couple of minutes of the first air exposure and stays stable after. The complete SEY/XPS results are given by tab. 4.3.

Table 4.3: XPS and SEY results of the measurements with and without bias voltage, results (a) correspond to the measurements after first conditioning, results (b) after second conditioning and results (c) after 19 days of air exposure wrapped in aluminium foil.

Sample	C [At%]	Cr [At%]	Fe [At%]	N [At%]	O [At%]	Si [At%]	SEY	total CD [C/mm^2]	second CD [C/mm^2]
ch 1 a	65.4	2.3	1.7	2.4	24.8	3.5	1.32	$2.18\,e^{-3}$	-
ch 8 a	70.7	1.7	1.9	2.4	20.4	2.8	1.30	$1.93\,e^{-3}$	-
ch 1 b	71.3	1.8	1.4	3.0	20.2	2.3	1.44	$3.34\,e^{-3}$	$1.16\,e^{-3}$
ch 8 b	46.6	4.5	5.1	1.8	39.1	3.1	1.27	$3.00\,e^{-3}$	$1.07\,e^{-3}$
ch 1 c	71.8	1.2	1.6	2.4	20.5	2.5	1.45	$3.34\,e^{-3}$	$1.16\,e^{-3}$
ch 8 c	50.3	2.4	2.5	1.6	37.7	5.5	1.34	$3.00\,e^{-3}$	$1.07\,e^{-3}$

4.2.5 Injection of Carbonaceous Gases during Multipacting runs with 1000 V Bias Voltage

Since the operation time of the accelerators is very expensive it is desired to reduce the time necessary for the conditioning of the accelerators' inner walls to a minimum. With this in mind, runs with acetylene (C_2H_2) and dodecane ($C_{12}H_{26}$) injection were carried out to accelerate the accumulation of carbon on the surface and therewith the conditioning process. Acetylene was chosen due to the good ratio between carbon and hydrogen and dodecane due to its high sojourn time. For the acetylene an injection pressure of 1×10^{-6} mbar and for the dodecane a pressure of 2×10^{-6} mbar compared to a base pressure of low 10^{-7} to high 10^{-8} mbar were chosen.

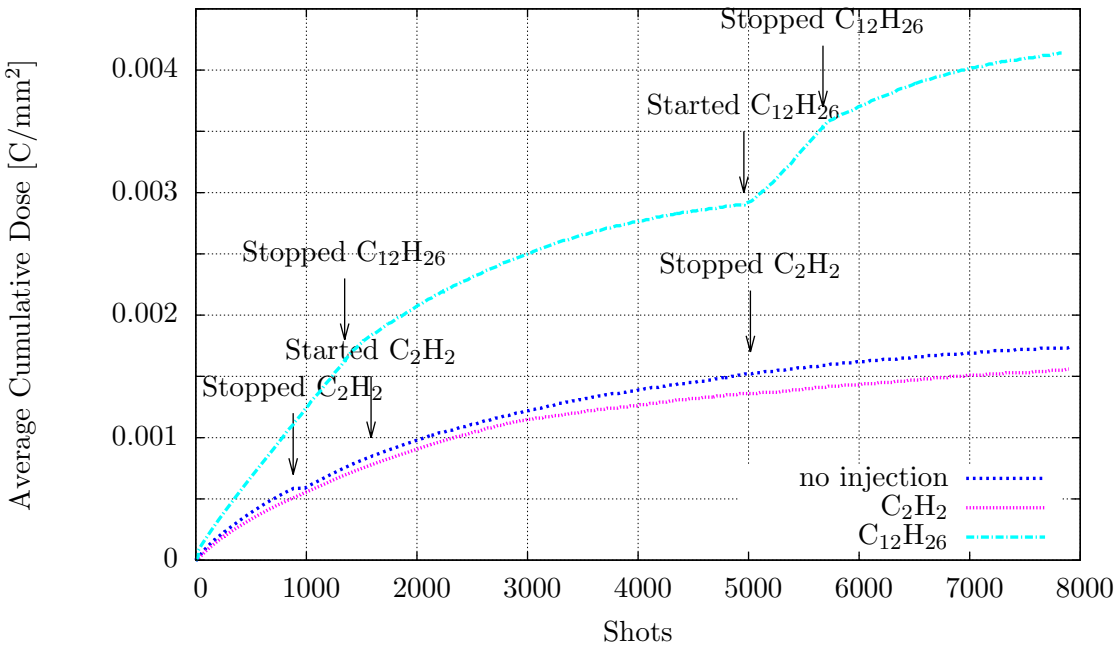

Figure 4.19: Cumulative dose during three Multipacting runs with 1000 V bias voltage, one without injection of carbonaceous gases, one with injection of acetylene and one run with injection of dodecane, acquired with transversal stripe detector.

Fig. 4.19 shows the average cumulative dose and fig. 4.20 shows the average dose per shot both as a function of the number of shots for a run without gas injection, for a run with dodecane injection and for a run with acetylene injection. In case of the run with acetylene injection no changes in the Multipacting behaviour compared to the run without injection were observed. Furthermore the average dose did not show any changes due to starting and stopping the injection. The dodecane on the other hand enhanced the Multipacting and lead therefore to an average cumulative dose of more than two times the one of a run without injection. During the injection of the dodecane the dose per shot showed the usual exponential decay, but reached a stable value one order of magnitude higher compared to a run without dodecane. After stopping the injection the dose per shot decreased rapidly and approached the same values as in the run without injection. Injection of dodecane for a second time lead again to an increase in the dose per shot and recovered the previous value during injection. This behaviour can be explained by an increase in the SEY due to the fresh dodecane layer continuously adsorbed on the liner's surface. This is also consistent with the effect of airborne contamination on the SEY and the high SEY of polymers.

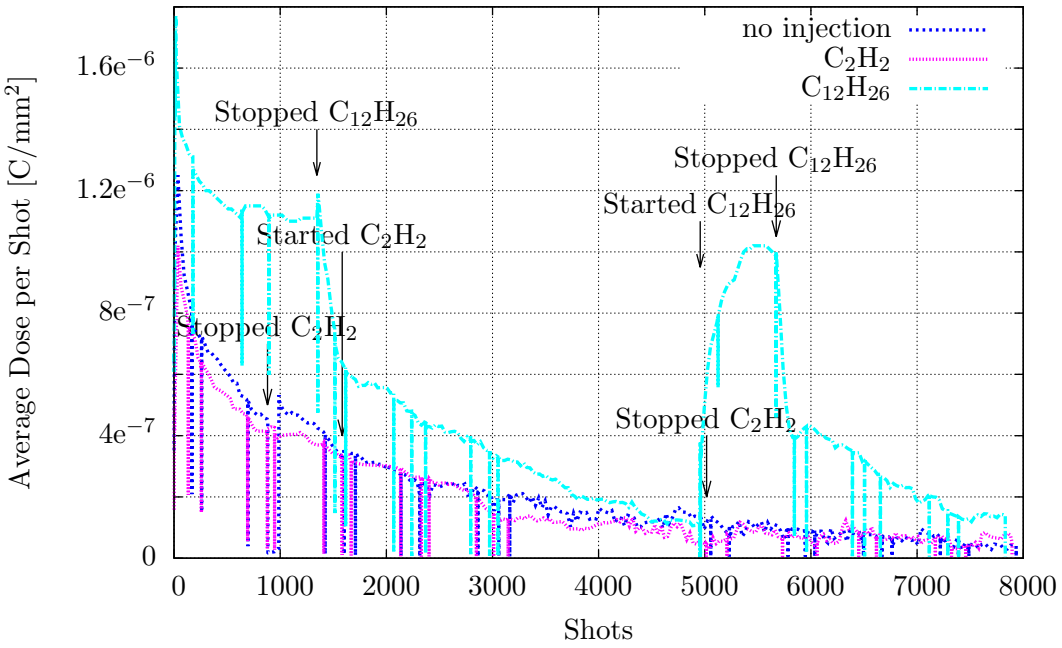

Figure 4.20: Development of the dose per shot during three Multipacting runs with 1000 V bias voltage, one without injection of carbonaceous gases, one with injection of acetylene and one run with injection of dodecane, acquired with the transversal stripe detector.

During the measurement runs with gas injection RGA measurements during single shots were applied. Fig. 4.21 and 4.22 show such RGA scans. In the case of the three shots applied during acetylene injection one sees a strong increase for the masses 24, 25, 26 and 27, these are the masses related to acetylene and its cracked molecule fragments. Furthermore, a higher amount of carbonmonoxide (28,29) and methane (16) was detected even though the H_2 increased with and without acetylene by the same amount. During the run with acetylene no Hydrocarbons related to the masses 37-43 were observed due to a probably initially cleaner surface of the liner.

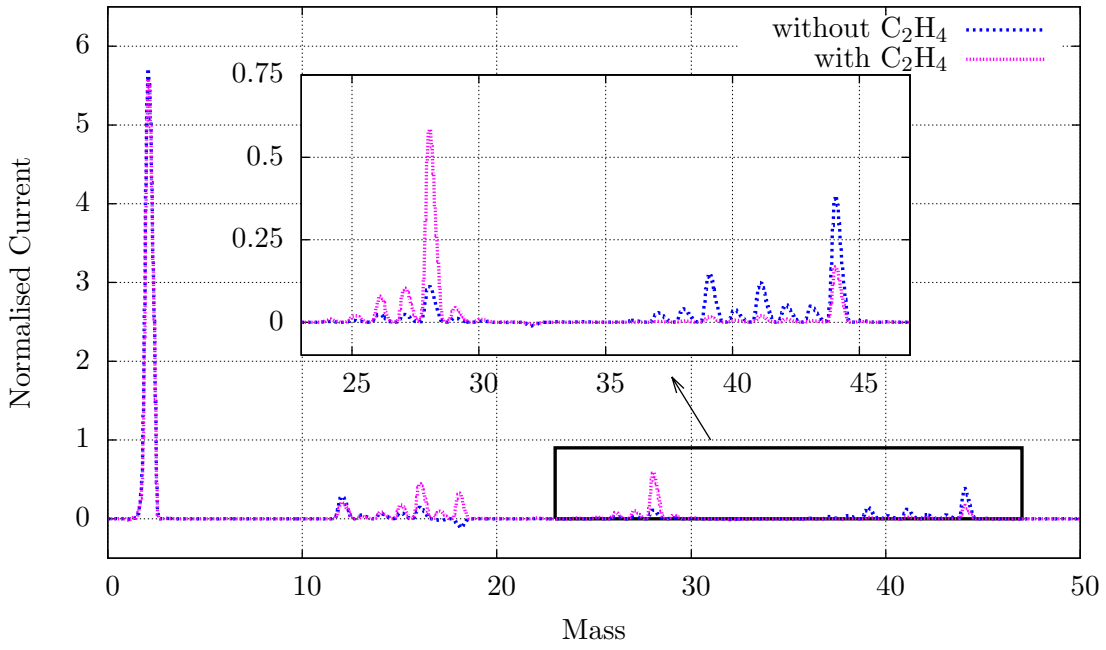

Figure 4.21: Normalised RGA scan with a SEM voltage of 1200 V of a shot from a run without and with C_2H_2 injection after baseline subtraction.

Fig. 4.22 shows the RGA measurements of three shots in between dodecane injection and three shots during dodecane injection. The RGA showed a loss of sensitivity due to the dodecane. This might be caused by an SEY decrease of the SEM due to dodecane adsorbates on the SEM's surface. In between dodecane injection the main gases released due to the electron stimulated desorption are, as in a normal run, molecular hydrogen (2) and carbonmonoxide (28). Furthermore, during Multipacting an increase in CO_2 (44) and C (12) was observed. During dodecane injection masses up to 84 were observed. All masses but molecular hydrogen (2) seemed to maintain stable during the Multipacting, this might be due to the high dodecane partial pressure of 2×10^{-6} mbar, which dominates the spectrum.

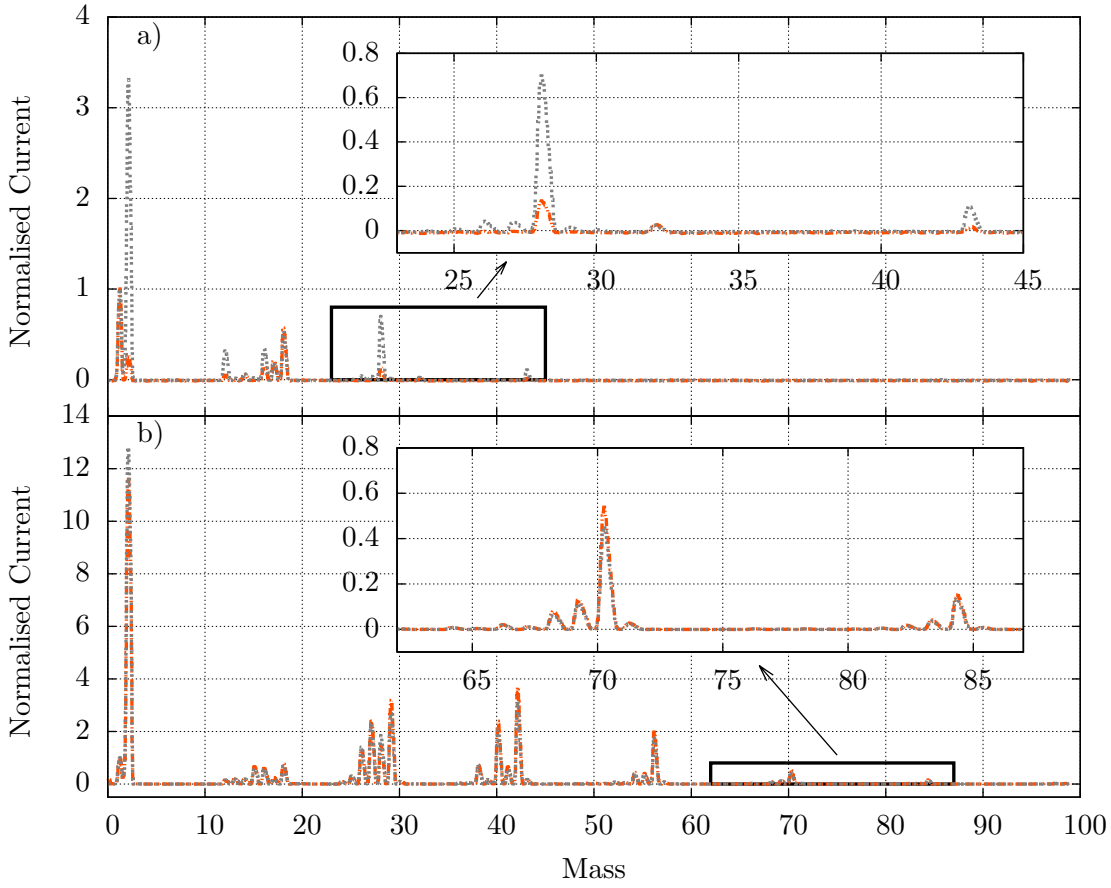

Figure 4.22: Normalised RGA spectra of two shots from the run with dodecane injection, a) in between dodecane injection and b) during dodecane injection before(orange) and during (grey) Multipacting (SEM voltage 1200 V, no background was subtracted).

The SEY/XPS results of the samples extracted after the run with acetylene injection showed a high SEY of 1.69 (CD 1.77×10^{-3}) in the front and 1.41 (CD 1.56×10^{-3}) in the rear of the liner compared to the values achieved without injection of 1.29 (CD 1.54×10^{-3}) and 1.26 (CD 3.95×10^{-3}). An interesting observation was also that the carbon concentration in the front of the liner is only 46.2 At%. Therefore, it seems as if the acetylene injection was not able to increase the accumulation of carbon on the liner's surface, since a decrease was in fact observed. An explanation for the removal of the carbon might be that during the Multipacting hydrogen and/or oxygen radicals are built and react with the carbon on the surface of the liner to CO and CH_4. Since the acetylene was injected during the beginning of the measurement run while the e-cloud was located in the front of the liner the carbon was mainly removed there.

For the run with dodecane injection the SEY/XPS results showed a very low SEY of 1.25 and a carbon concentration of 92.6 At% in front of the liner, but a rather high SEY of 1.43 with a much lower carbon concentration of 60.4 At% in the rear. This might be due to a completely different e-cloud distribution during the injection of dodecane. During the injection the e-cloud was concentrated in the front and middle of the liner and only moved to the rear in between and after injection. The complete SEY/XPS results are given by tab. 4.4.

Table 4.4: XPS and SEY results of the measurements with and without injection of acetylene and dodecane at channel 1 and 16, a bias voltage of 1000 V was applied during every run.

Sample	C [At%]	Cr [At%]	F [At%]	Fe [At%]	N [At%]	O [At%]	SEY_{max}	CD [C/mm^2]
only bias Ch1	75.4	3.7	-	2.5	2.1	16.4	1.29	$1.54\,e^{-3}$
C_2H_2 Ch1	46.2	9.2	2.2	6.7	1.7	34.0	1.69	$1.77\,e^{-3}$
$C_{12}H_{26}$ Ch1	92.6	-	-	-	0.7	6.7	1.25	$8.27\,e^{-3}$
only bias Ch16	79.7	1.7	-	1.5	3.5	13.5	1.26	$3.95\,e^{-3}$
C_2H_2 Ch16	80.1	2.3	-	1.4	1.8	14.4	1.41	$1.56\,e^{-3}$
$C_{12}H_{26}$ Ch16	60.4	6.6	-	5.9	2.2	25.0	1.43	$4.38\,e^{-3}$

The C1s lines of a run without gas injection, with acetylene injection, dodecane injection and a carbon coating with 0.007 % H_2 are given by fig. 4.23. In case of the C1s line of the carbon coating 0.1 eV were subtracted from the binding energy in order to overlap the line with the one of the dodecane run. The C1s line of the run with acetylene showed a very similar shape as the C1s line of the run without injection. The sample of the measurement run with dodecane injection on the other hand showed a completely different behaviour. As the C1s line showed a very steep decrease on the high binding energy side even though the sample was featured with an SEY of 1.26. However, the comparison of the C1s line of a carbon coating with a very similar SEY of 1.27 showed great similarity. The carbon deposited on the surface during dodecane injection changed from the behaviour of a conditioned sample to the behaviour of a carbon coated sample with hydrogen injection. Therefore, in this case, the main factor might not be the cumulative dose, but the amount of hydrogen present in the residual gas, which is strongly affected by the hydrogen released due to the cracking of the dodecane molecules or by the amount of hydrogen remaining within the cracked dodecane molecules which are forming the carbon layer.

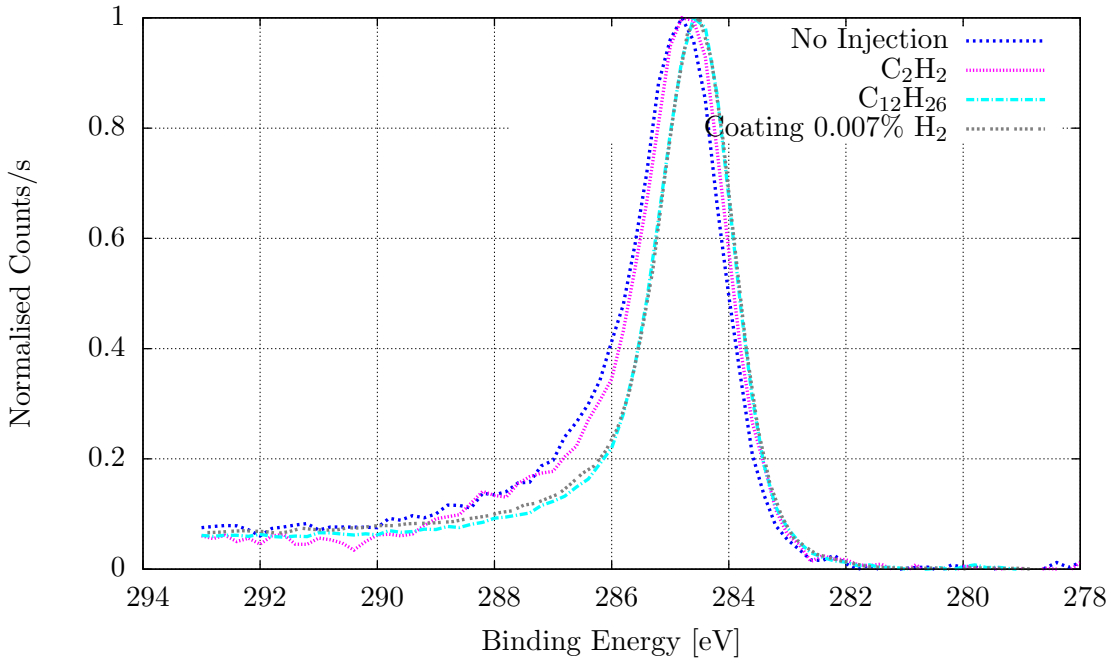

Figure 4.23: The normalised C1s lines of the measurements without injection of hydrocarbons, with injection of acetylene or dodecane and a carbon coating with 0.7 % H_2 in the working gas (binding energy -0.1 eV).

4.3 Conclusion and Future Outlook

Multipacting represents a limiting factor for modern days accelerators. Therefore, different techniques to mitigate Multipacting are investigated, one of these techniques, the reduction of the SEY of the surface through surface conditioning was studied in the present work. It was shown that superimposing an RF signal with a positive DC bias voltage enhances the Multipacting, probably due to an increase of the electron energy. Since it was possible to acquire higher cumulative doses with the DC bias voltage it was possible to lower the resulting SEY in the rear of the liner after 11 days of conditioning from 2.23 to 1.33. Hence, it was also shown that it is possible to reach an SEY below the threshold value for Multipacting in the SPS. Furthermore, a dynamic behaviour of the e-cloud during the measurements was observed, which reflected the progress in the surface conditioning and showed significant differences between measurements with and without the DC bias voltage. Measurement runs with injection of dodecane and acetylene in order to accelerate the conditioning were carried out. These measurements proved the injection of acetylene and dodecane as unsuitable to accelerate the condition-

ing in particle accelerators. Moreover, studies on the effect of air exposure showed that the remaining effect of the conditioning after exposure to air depends on the thickness of the carbon layer on top and therewith on the received cumulative dose.

In order to also transfer the knowledge gained with the Multipacting test bench to the LHC additional measurements using copper instead of stainless steal liners have to be carried out. The measurement of carbon coated liners with different SEY is planned in order to find the threshold SEY of the Multipacting test bench and to determine the threshold power for Multipaciting for different SEYs. Studies with an improved vacuum system are foreseen in order to better understand the role of the residual gas during the measurement run. Furthermore, computer simulations of the e-cloud build up in the Multipacting test bench could help to better understand the dynamic of the electron cloud and the effect of the DC bias voltage.

Bibliography

[1] V. Baglin et al. "The secondary electron yield of technical materials and its variation with surface treatments". In: *LHC Project Report 433* (2000).

[2] Vincent Baglin. "HL-LHC: What is it and what challenges it represents for VSC". In: (5-12-2014).

[3] J. L. Baldy et al. "Site Layout of the propsed new hadrons' injector chain at CERN". In: *CERN-AB-2008-061* (2008).

[4] Amadeo Bellunato. "Experimental Investigation on the Electron Multipacting and the Surface Conditioning". Masterthesis, Politecnico di Milano. 2014.

[5] *Bonding and Hybridization*. URL: https://chemistry.boisestate.edu/richardbanks/inorganic/bonding%20and%20hybridization/bonding_hybridization.htm (visited on 11/11/2014).

[6] O. Brüning et al. "Multipacting Tests with Magnetic Field for the LHC Beam Screen". In: *LHC Project Report 187* (1998).

[7] *Carbon*. URL: http://www.chemistryexplained.com/elements/A-C/Carbon.html (visited on 11/11/2014).

[8] *CH 106 - Lesson 2*. URL: http://dl.clackamas.cc.or.us/ch106-02/typesof.htm (visited on 11/12/2014).

[9] R. Cimino et al. "Nature of the Decrease of the Secondary-Electron Yield by Electron Bombartment and its Energy Dependence". In: *Physical Review Letters PRL 109* (2012).

[10] *Diamond-based mircroplasmas*. URL: http://www.chm.bris.ac.uk/pt/diamond/microplasma.htm (visited on 04/14/2014).

[11] *Electron cloud*. URL: http://www.arturostabile.com/research-2.html (visited on 04/10/2014).

[12] *Following protons on a trip to (and through) the LHC*. URL: http://arstechnica.com/science/2010/08/following-protons-on-a-trip-to-and-through-the-lhc/ (visited on 08/21/2014).

[13] F.Zimmermann. "Review of single bunch instabilities driven by an electron cloud". In: *Physical Review Special Topics - Accelerators and Beams 7, 124801* (2004).

[14] Jang-Hui Han, Klaus Flöttmann, and Walter Hartung. "Single-side electron multipacting at the photocathode in rf guns". In: *Physical Review Special Topics - Accelerators and Beams 11, 013501* (2008).

[15] B. Henrist et al. "The variation of the secondary electron yield and of the desorption yield of copper under electron bombardment: origin and impact on the conditioning of the LHC". In: *EPAC 2002, Paris, France* (2002).

[16] *Hollow Cathode*. URL: http://www.exciton.biz/html/hollow_cathode.html (visited on 04/15/2014).

[17] Shigeki Kato and Michiru Nishiwaki. "Study on Graphitization and DLC Coating on KEKB LER Chambers". In: (12-10-2009).

[18] H. Koch et al. "Hollow cathode discharge sputtering device for uniform large area thin film deposition". In: *Journal of Vacuum Science & Technology A 9, 2374* (1990).

[19] *LUNAR DUST GRAIN CHARGING BY ELECTRON IMPACT: COMPLEX ROLE OF SECONDARY ELECTRON EMISSIONS IN SPACE ENVIRONMENTS*. URL: http://iopscience.iop.org/0004-637X/718/2/795/article (visited on 05/19/2014).

[20] M. Mattes, E. Sorolla, and F. Zimmermann. "Modeling microwave/electron-cloud interaction". In: *arXiv:1310.0212v1 [physics.acc-ph]* (2013).

[21] Renzo F. Parodi. "Multipacting". In: *arXiv:1112.2176 [physics.acc-ph]* (2010).

[22] F. Le Pimpec et al. "Electron conditioning of technical aluminium surfaces: Effect on the secondary electron yield". In: *Journal of Vacuum Science & Technology A 23, 1610* (2005).

[23] P. Costa Pinto et al. "Carbon coating of the SPS dipole chambers". In: *Proceedings of ECLOUD12* (2012).

[24] *Principles of Hollow Cathode Magnetron Sputtering Sources*. URL: http://www.isofluxinc.com/custFiles/files/Principles-and-Applications-of-Hollow-Cathode-Magnetron-Sputtering-Sources.pdf (visited on 04/14/2014).

[25] C. Scheuerlein and M. Taborelli. "The assessment of metal surface cleanliness by XPS". In: *Applied Surface Science 252 (2006) 4279-4288* (2005).

[26] C. Scheuerlein et al. "An AES study of the room temperature conditioning of technological metal surfaces by electron irradiation". In: *Applied Surface Science 202 (2002) 57-67* (2002).

[27] E. Shaposhnikova et al. "Experimental Studies of Carbon Coatings as Possible Means of Supressing Beam Induced Electron Multipacting in the CERN SPS". In: *CERN-AB-2008-061* (2008).

[28] A. Shih et al. "Secondary electron emission studies". In: *Applied Surface Science 111, 251-258* (1996).

[29] A. M. Shroff and J. C. Tonnerre. "Secondary electron emission". In: *Electron Devices Meeting, 1989. IEDM '89. Technical Digest., International* (1989).

[30] R. E. Simon and B. F. Williams. "Secondary electron emission". In: *Nuclear Science, IEEE Transactions on (Volume:15 , Issue: 3)* (1968).